LUT
Lappeenranta
University of Technology

Mei Han

# HYDRODYNAMICS AND MASS TRANSFER IN AIRLIFT BIOREACTORS: EXPERIMENTAL AND NUMERICAL SIMULATION ANALYSIS

Thesis for the degree of Doctor of Science (Technology) to be presented with due permission for public examination and criticism in Auditorium 2310 at Lappeenranta University of Technology, Lappeenranta, Finland on the 19th of December, 2017, at noon.

Acta Universitatis
Lappeenrantaensis 783

Supervisors Professor Tuomas Koiranen
LUT School of Engineering Science
Lappeenranta University of Technology
Finland

Docent Arto Laari
LUT School of Engineering Science
Lappeenranta University of Technology
Finland

Reviewers Professor Ville Alopaeus
Department of Chemical and Metallurgical Engineering
Aalto University
Finland

Associate Professor Ronnie Andersson
Department of Chemical Reaction Engineering
Chalmers University of Technology
Sweden

Opponent Professor Ville Alopaeus
Department of Chemical and Metallurgical Engineering
Aalto University
Finland

Custos Professor Tuomas Koiranen
LUT School of Engineering Science
Lappeenranta University of Technology
Finland

ISBN 978-952-335-188-2
ISBN 978-952-335-189-9 (PDF)
ISSN-L 1456-4491
ISSN 1456-4491

Lappeenrannan teknillinen yliopisto

Yliopistopaino 2017

# ABSTRACT

Mei Han

## Hydrodynamics and mass transfer in airlift bioreactors: experimental and numerical simulation analysis

Lappeenranta 2017
72 p.

Acta Universitatis Lappeenrantaensis 783
Diss. Lappeenranta University of Technology

ISBN 978-952-335-188-2, ISBN 978-952-335-189-9 (PDF),
ISSN-L 1456-4491, ISSN 1456-4491

Airlift bioreactors are widely used in industrial applications such as wastewater treatment, gas decontamination and other biochemical processes, and such systems have generated increasing academic and industrial interest. Many bioprocesses occurring in airlift bioreactors are limited by the gas-liquid mass transfer, which is determined by the hydrodynamics of the multiphase flow. The hydrodynamics of multiphase flow in airlift bioreactors is complex and involves a large number of interrelated hydrodynamic parameters that are influenced by factors such as aeration mode, liquid physical properties and reactor scale. In study of bioreactor performance, detailed numerical data on local hydrodynamics, which is crucial for design of multiphase reactors and optimization of operating conditions, is often limited by available measurement techniques. Furthermore, while many simulation studies of airlift reactors have been reported for Newtonian fluids, there is a lack of numerical simulation study of airlift bioreactors incorporating the non-Newtonian fluid rheology commonly encountered in bioprocesses.

The aim of this thesis is to improve understanding of the hydrodynamic and mass transfer performance of airlift bioreactors and thereby contribute to their improved application, design and scale-up, as well as optimization of aeration. Both experimental and numerical simulation approaches are used in the research work.

In the thesis work, novel and advanced measurement techniques – three-dimensional electrical impedance tomography and particle image velocimetry – were applied in the

experimental studies, together with conventional methods. The experimental results bring better understanding of the hydrodynamics of industrial airlift bioreactors.

Detailed quantitative analysis of local hydrodynamics and mass transfer characteristics of center- and annulus-rising airlift bioreactors was performed, which provided important insights into the effect of the aeration mode on airlift bioreactor performance. Experimental results presented in the thesis facilitate the design and effective utilization of airlift reactors, particularly for biochemical applications, by providing valuable information about key phenomena such as local flow structure, shear rate field and foam layer thickness.

Investigation of gas distribution and local gas holdup was carried out using tomographic imaging techniques with non-Newtonian fluids commonly encountered in industry. Novel experimental results of visualized gas distribution are presented, bringing new insights into potential approaches for improvement of aeration and effective gas-liquid contact. Better understanding of the effect of the hydrodynamics on mass transfer was achieved by separation of the liquid-side mass transfer coefficient and the gas-liquid interfacial area.

Numerical simulation results of the three-phase model comprising the liquid phase and two gas bubble phases developed in this work are presented and compared with experimental results from both this study and published literature. Comparison of the experimental and simulation results showed that the developed three-phase model is capable of predicting well the hydrodynamics and mass transfer for low viscous fluids over the three circulation flow regimes studied. The effects of the reactor scale are predicted reasonably well. To give more confident prediction for airlift bioreactors with viscous non-Newtonian fluids, a computational fluid dynamic model with wide bubble size distribution due to bubble breakage and coalescence was developed and used in simulations with ANSYS Fluent Solver in homogeneous and heterogeneous flow regimes. Good agreement between the experimental and simulated results indicated that the developed computational fluid dynamic model is able to describe and predict the hydrodynamics in airlift bioreactors with non-Newtonian fluids with reasonable accuracy.

**Keywords:** Airlift bioreactor, Hydrodynamics, Mass transfer, Particle image velocimetry, Electrical impedance tomography, Model development, Computational fluid dynamics, Population balance model

# ACKNOWLEDGEMENTS

This research work was carried out in the School of Engineering Science at Lappeenranta University of Technology.

I express my deepest gratitude to my supervisors, Professor Tuomas Koiranen and Docent Arto Laari, for giving me the support and freedom to perform the research. I thank them for their invaluable advice and guidance throughout the work. I am very grateful to Professor Ilkka Turunen and Professor Zuoliang Sha, who gave me the opportunity to start my doctoral studies, and who introduced me to the world of scientific research.

I am also grateful to Professor Marko Vauhkonen at the Department of Applied Physics, University of Eastern Finland. His constructive advices greatly helped in the investigation of EIT measurements and analysis.

I gratefully thank Professor Ville Alopaeus and Associated Professor Ronnie Andersson for their valuable comments, which made it possible to improve the thesis. I thank Peter Jones for his hard work in language revision of the manuscripts and thesis.

The Graduate School of Chemical Engineering (GSCE), Outotec Oyj, the Finnish Funding Agency for Technology and Innovation (TEKES), and the FERMATRA Project are gratefully acknowledged for financial support of this research. I also acknowledge the CSC-IT Center for Science, Finland, for computational resources.

I thank my many colleagues and friends in Finland, especially Abayneh Demesa, Bing Han, Dmitry Gradov, Gerardo González, Ming Li, Vladimir Zhukov, Waroonkarn Srithammavut, Wenli Zhao, Yongbo Wang and Yuwei Bie, for their help, encouragement and friendship. We had many enjoyable discussions and shared many memorable moments in Finland. I would also like to thank my many friends outside Finland for their encouragement and friendship.

Finally, I express my greatest thanks to my family for their love and unwavering support.

*Mei Han*

December 2017, Lappeenranta, Finland

# TABLE OF CONTENTS

# LIST OF PUBLICATIONS

This thesis is based on the following publications, which are referred to in the text by Roman numerals I-IV.

I. **Han M**, Laari A., Koiranen T., Effect of aeration mode on the performance of center- and annulus-rising internal-loop airlift bioreactors, Canadian Journal of Chemical Engineering, 2017. In Press.

II. **Han M**., González G., Vauhkonen M., Laari A., Koiranen T., Local gas distribution and mass transfer characteristics in an annulus-rising airlift reactor with non-Newtonian fluid, Chemical Engineering Journal, 2017, Vol. 308, 929-939.

III. **Han M**, Laari A., Koiranen T., Hydrodynamics and mass transfer performance of annulus-rising airlift reactor – the effect of reactor scale, International Journal of Chemical Engineering and Applications, 2017, Vol. 8, 47-52.

IV. **Han M**., Sha Z.L., Laari A., Koiranen T., CFD-PBM coupled simulation of an airlift reactor with non-Newtonian fluid, Oil & Gas Science and Technology – Revue d'IFP Energies nouvelles, 2017, Vol. 72, 1-12.

## Author's contribution to the publications

The author was the primary contributor in publications I - IV. For Publication I, the author carried out the experiments and analyzed the results. The author wrote the paper with the co-authors. For Publication II, the author designed and carried out the experiments. The author analyzed the EIT measurement result and wrote the paper with the co-authors. For Publication III, the author carried out the experiments and the simulations and analyzed the results. The author was responsible for the model development and wrote the paper with the co-authors. For Publication IV, the author carried out the experiments and model development and wrote the paper with the co-authors.

In addition to the publications listed above, the author has also presented related work at three scientific conferences.

## Related Conference Presentations

I. **Han M.**, Laari A., Turunen I., Sha Z.L., CFD simulation and PIV validation of air-liquid flow in the center-ring airlift reactor, 9th World Congress of Chemical Engineering, August 18-23, 2013, Seoul, South Korea, Oral presentation.

II. **Han M.**, Laari A., Sha Z.L., Turunen I., CFD simulation and PIV validation of bubbly flow in an internal-loop airlift reactor, 17th Conference on Process Integration, Modelling and Optimization for Energy Saving and Pollution Reduction, August 23-27, 2014, Prague, Czech Republic, Poster presentation.

III. **Han M.**, Laari A., Sha Z.L., Koiranen T., Turunen I., A study of internal-loop airlift bioreactor hydrodynamics by CFD simulations and Particle Image Velocimetry measurements, 3rd Finnish Symposium and Summer School on Reaction Engineering, June 14-18, Lapland, Finland, Oral presentation.

# List of symbols and abbreviations

## Symbols

| | |
|---|---|
| $a$ | Gas-liquid interfacial area, $m^2/m^3$ |
| $A_d$ | Cross-sectional area of downcomer, $m^2$ |
| $A_r$ | Cross-sectional area of riser, $m^2$ |
| $b_i$, $b(d)$ | Specific bubble breakup rate due to turbulent fluctuation, 1/s |
| $b_{in}$ | Bubble breakup rate due to instability, 1/s |
| $b^*$ | Model parameter for bubble breakup due to instability,- |
| $c$ | Bubble coalescence rate, $m^3/s$ |
| $C_{sensor}$ | Dissolved oxygen concentration indicated by sensor, mg/L |
| $C^*$ | Oxygen saturation concentration, mg/L |
| $d$ | Bubble size, m |
| $d_c$ | Critical bubble size for bubble breakup due to instability, m |
| $d_{cw}$ | Critical bubble size for bubble coalescence due to wake entrainment, m |
| $d_{32}$ | Bubble Sauter mean diameter, mm |
| $f_i$ | Volume fraction in gas holdup of bubble group $i$, - |
| $f_v$ | Bubble breakup fraction, - |
| $h$ | Axial position from gas distributor in the AR-ALR, m |
| $h_0$ | Initial film thickness between two coalescing bubbles, m |
| $h_f$ | Critical film thickness between two coalescing bubbles, m |
| $k$ | Turbulence kinetic energy, $m^2/s^2$ |
| $k_L$ | Liquid-side mass transfer coefficient, m/s |
| $k_La$ | Volumetric mass transfer coefficient per unit volume of reactor, 1/s |
| $l$ | Largest eddy size effective to bubble breakup, m |
| $m$ | Model parameter for bubble breakup due to instability , - |
| $n$ | Flow index, - |

| | |
|---|---|
| $P$ | Bubble coalescence efficiency, - |
| $P_b$ | Probability density function, - |
| $r$ | Bubble radius, m |
| $r_{ij}$ | Equivalent radius defined as $r_{ij}=1/(2(1/r_i+1/r_j))$, m |
| $R$ | Radial coordinate, m |
| $St$ | Bubbl Stokes number, |
| $\bar{u}_\lambda$ | Average velocity of eddy of size λ, m/s |
| $U_c$ | Liquid circulation velocity, m/s |
| $U_g$ | Superficial gas velocity, cm/s |
| $v$ | Bubble volume, $m^3$ |
| $We$ | Weber number, $\rho d u^2/\sigma$ |

## Greek symbols

| | |
|---|---|
| $\alpha$ | Phase fraction, - |
| $\beta$ | Daughter bubble size distribution function, - |
| $\gamma$ | Shear rate, 1/s |
| $\Gamma_{i,j}$ | Coefficient related to the bubble distance,- |
| $\delta$ | Kronecker delta function, - |
| $\varepsilon$ | Turbulence kinetic energy dissipation rate, $m^2/s^3$ |
| $\eta_{i,k}$ | Distributing coefficient related to bubble breakup,- |
| $\theta$ | Model parameter in kernel model of bubble breakup due to turbulent fluctuations, - |
| $\Theta$ | Coefficient related to the critical bubble size $d_c$,- |
| $\kappa$ | Consistency index, Pa $s^n$ |
| $\lambda$ | Eddy size, m |
| $\mu_{app}$ | Apparent viscosity, Pa s |
| $\xi_{ij}$ | Ratio of bubble sizes defined as $d_i/d_j$, - |
| $\rho$ | Density, $kg/m^3$ |
| $\sigma$ | Surface tension, N/m |
| $\tau$ | Relaxation time, 1/s |

| | |
|---|---|
| $\psi_{i,k}$ | Distributing coefficient related to bubble breakup,- |
| $\omega$ | Bubble collision frequency, $m^3/s$ |

## Subscripts

| | |
|---|---|
| *b* | Bubble |
| *C* | Coalescence |
| *f* | Fluid |
| *g* | Gas phase |
| *i, j, k* | Bins/groups of bubble size |
| *L* | Liquid phase |
| *slip* | Slip velocity |
| *S* | Shear |
| *T* | Turbulent fluctuations |
| *U* | Bubble rise velocity |
| *W* | Wake |

## Abbreviations

| | |
|---|---|
| ALR | Airlift reactor |
| IL-ALR | Internal-loop airlift reactor |
| EL-ALR | External-loop airlift reactor |
| CR-ALR | Center-rising airlift reactor |
| AR-ALR | Annulus-rising airlift reactor |
| PIV | Particle image velocimetry |
| EIT | Electrical impedance tomography |
| CFD | Computational fluid dynamics |
| PBM | Population balance model |

# 1. Introduction

## 1.1 Background

Airlift reactors (ALRs) are widely used in the chemical, petrochemical, biochemical and environmental industries for processes such as acetophenone hydrogenation (Bergault *et al*., 1999), direct coal liquefaction (Huang *et al*., 2015), syngas fermentation (Munasinghe *et al*., 2015), wastewater purification (Heijnen *et al*., 1997) and exhaust-gas treatment (Jafari Nasr *et al.*, 2004). ALRs exhibit superior performance to traditional bubble columns, including higher mass and heat transfer, enhanced mixing efficiency and good suspension of solids with low power input. Compared to mechanically stirred tanks, their simple structure, mild shear stresses and low energy consumption make ALRs even more attractive, especially for bioprocesses with fragile particles (Chisti, 1989). These advantages of ALRs have generated increasing academic and industrial interest, particularly in view of current stringent energy and safety demands.

Many bioprocesses in airlift bioreactors are limited by the mass transfer of sparingly soluble gaseous reactants, and this constraint has been considered as the main impediment to commercialization of some green chemical and biochemical technologies (Munasinghe *et al*., 2015), e.g., syngas (industrial tail gas) fermentation. Gas-liquid mass transfer in ALRs is substantially determined by the hydrodynamics of the multiphase flow. The hydrodynamics of multiphase flow is complex and still not fully understood for ALRs, particularly for culture media commonly found in typical bioprocesses. Many of the hydrodynamic parameters are interrelated, and they are affected by factors such as aeration mode, liquid physical properties and reactor scale.

Process solutions in fermentation often contain organic compounds, such as alcohols or organic acids, as carbon source, nutrients and microbial biomass. Organic compounds and nutrients are surface-active compounds that tend to hinder bubble coalescence and thus influence in bubble size, gas-liquid interfacial area and gas-liquid mass transfer. Foaming is also often a problem during fermentation, and antifoaming agents are commonly added

to reduce excessive foaming. Addition of antifoaming agents, on the other hand, intensifies bubble coalescence. Therefore, surface activity in fermentation media is often very complex and evaluation of mass transfer parameters from literature correlations has high uncertainty. Consequently, these parameters are usually evaluated experimentally. Moreover, knowledge of local detailed hydrodynamic information is crucial for effective reactor design, scale-up and process optimization. However, information on local hydrodynamics is often limited by available measurement techniques. Furthermore, there is a lack of numerical simulation studies that take into account the complex bubble hydrodynamics of the non-Newtonian fluids commonly encountered in bioprocesses (Chavez-Parga *et al.*, 2007; Chavez-Parga *et al.*, 2008; Lennartsson *et al.*, 2011).

### 1.1.1 Airlift reactors

The concept of the ALR was proposed and patented by Le Francois (Berovic, 2009) in 1955. ALRs are a type of pneumatically agitated bioreactor in which the gaseous phase functions as the agitation source and, in most cases, is the reactant. The three main parts of the ALR are the riser, the downcomer and the gas distributor. In ALR operation, the gas is fed into the riser, and the liquid flows upwards in the riser and downwards in the downcomer. In cases where the gas needs to be well separated from the liquid, an enlarged expansion, called a gas separator, is placed at the top of the reactor. Based on the arrangement of the riser and the downcomer, ALRs are generally categorized into two classes: internal-loop airlift reactors (IL-ALR) and external-loop airlift reactors (EL-ALR). Two aeration modes can be operated in an IL-ALR: gas feed in the draft tube (a center-rising airlift reactor, CR-ALR) and gas feed in the annulus between the draft tube and the outer column (an annulus-rising airlift reactor, AR-ALR).

The hydrodynamics in an ALR is characterized by two flow regimes: homogeneous flow (bubbly flow) and heterogeneous flow (churn-turbulent flow). In homogeneous flow, bubble interactions are negligible and bubble size is narrowly distributed. The overall gas holdup increases remarkably with superficial gas velocity in homogeneous flow. In heterogeneous flow, which is encountered at high gas superficial velocities, bubble breakage and coalescence become pronounced and the bubble size distribution is broad.

In the heterogeneous flow regime, the overall gas holdup increases slightly with increasing superficial gas velocity.

Three circulation flow regimes have been defined for ALRs (Heijnen *et al*., 1997; Blažej *et al*., 2004) based on bubble entrainment in the reactor. In circulation flow regime I, no gas is entrained in the downcomer; in circulation regime II, small bubbles are entrained into downcomer but there is no recirculating into the riser; and in regime III, there is substantial recirculation of bubbles into the riser. Research work using laboratory-scale ALRs generally focuses on circulation regimes I and II. Circulation regime III, which commonly occurs in full-scale ALRs, is often difficult to attain in laboratory-scale equipment (Heijnen *et al*., 1997), mostly due to the relatively low liquid circulation velocity.

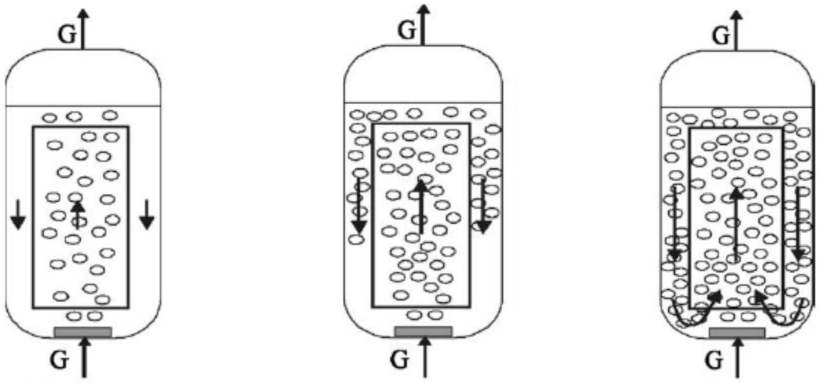


(a) (b) (c)

Figure 1. Circulation flow regimes in ALRs: (a) regime I, (b) regime II, (c) regime III (Blažej *et al*., 2004).

### 1.1.2 Measurement techniques

The measurement techniques used play a very important role in investigation of the hydrodynamics and mass transfer in ALRs. The depth of experimental study is directly determined by the measurement scope, accuracy, significance and reliability. Recently, a number of advanced measurement techniques have been introduced and applied in hydrodynamic studies, for example, radioactive particle tracking and electrical resistance tomography (Luo and Al-Dahhan, 2008, 2010; Gumery *et al.*, 2011). However, much

more work is still needed. Based on the spatial characteristics of the measured hydrodynamics, applicable measurement techniques can be classified into two categories – global and local hydrodynamics measurements. Next, typical global and local hydrodynamics measurement techniques are briefly introduced and summarized in Table 1.

Global hydrodynamics measurements

**Bed expansion** Bed expansion, also called height or volume expansion, is a conventional method to measure the overall gas holdup in gas-liquid multiphase reactors. The gas holdup in the reactor is measured by comparing the liquid levels before and after aeration. Many researchers (Zhang *et al*., 2002; Luo and Al-Dahhan, 2010) have used this method to investigate overall gas holdup in airlift reactors. The bed expansion method cannot be used when the upper surface of the liquid is remarkably unstable at high gas superficial velocity.

**Differential pressure drop** Differential pressure drop is commonly used to measure average gas holdup in airlift reactors (Klein *et al*., 2003; van Baten *et al*., 2003). The pressure drop is measured with a U-tube manometer or pressure transmitter. This conventional measurement method has been used to examine and verify the accuracy of other measurement methods and novel measurement techniques (Wu *et al*., 2009). Only volumetric averaged gas holdup can be measured using the differential pressure drop method.

**Liquid solution tracer** A liquid solution tracer can be used to measure the bulk liquid circulation velocity and average liquid velocity in airlift reactors (Zhang *et al*., 2002; van Baten *et al*., 2003; Vial *et al*., 2002). In the approach, a salt or acid solution is introduced from the bottom of reactor and the peak pulse of conductivity or pH is detected using a conductivity probe or pH meter at the top of the reactor. The bulk circulation velocity and average liquid velocity can be calculated from the detected peak pulses and the distance between the probe and the tracer injection locations. The accuracy of this method is often low due to the short equilibrium time of the tracer concentration.

Local hydrodynamics measurements

**Hot-film anemometry (HFA)** HFA can be used to measure the instantaneous velocities and turbulence characteristics of liquid flows in airlift reactors (Ali *et al.*, 2011). This method is based on the dependence of the sensor heat transfer on the liquid velocity, temperature and composition. HFA measurement gives single-point information, and for effective use, the HFA method requires a constant temperature environment.

**Digital imaging** Digital imaging or photography methods can be used to evaluate gas holdup, bubble size and size distribution, and even bubble rise velocity (Vial *et al.*, 2002; Liu *et al.*, 2011a). Digital imaging methods are limited by the system transparency and difficulties in detection of overlapping bubbles.

**Probe techniques** Probe techniques mainly comprise optical and electrical resistivity measurement and give single-point measurement results. Probe techniques have been used to investigate characteristics of bubble dynamics in airlift reactors (Wu *et al.*, 2009; Lo and Hwang, 2003; Deng *et al.*, 2010), e.g., local gas holdup, bubble rise velocity, and bubble size and size distribution. Probe techniques are usually limited by the assumption that bubbles are spherical or ellipsoidal in shape.

**Laser Doppler Velocimetry (LDV)** LDV can be used to measure local gas velocity, liquid velocity and turbulence characteristics (Vial *et al.*, 2002). LDV is an optical measuring technique based on the Doppler effect of scattered light. The LDV technique gives single-point data and is limited by system transparency.

**Computed tomography (CT)** CT is able to measure local gas holdup and distribution in airlift reactors (Luo and Al-Dahhan, 2010). The measurements are obtained by detecting and analyzing the attenuation of ϒ-ray radiation caused by the gas phase in gas-liquid phase flow. The CT technique is generally expensive, and there are safety issues associated with use of this technique.

**Computer automated radioactive particle tracking (CARPT)** CARPT is a non-intrusive three dimensional flow field measurement technique. Time-averaged liquid hydrodynamics in the airlift reactor (Luo and Al-Dahhan, 2008), e.g., velocity field, shear

stress and turbulence characteristics, are obtained by tracking and analyzing a small radioactive particle that follows the liquid phase. Only time-averaged measurements are possible using the CARPT technique and appropriate safety measures are required.

**Particle Image Velocimetry (PIV)** PIV is a non-intrusive and non-interruptive optical measuring technique that gives full-field, detailed and instantaneous velocity field data (Wu and Merchuk, 2003). Based on the measured velocity, additional hydrodynamic (Fujiwara *et al.*, 2004; Lin and Chen, 2005) parameters can be obtained and analyzed, e.g. Reynold stresses. PIV measurement provides detailed experimental data for validation of computational fluid dynamics (Ge *et al.*, 2014). The PIV technique is limited by the system transparency and the need for high gas volume fraction.

**Electronic Resistance/Impedance Tomography (ERT/EIT)** ERT/EIT is a non-invasive tomographic imaging measurement technique based on estimation of the conductivity distribution (González *et al.*, 2015). ERT/EIT has the advantages of being real-time monitoring, at low-cost, and being capable of extracting local, detailed and visualized information. Local gas holdup, gas holdup distribution, gas velocity, mixing efficiency and liquid circulation time can be measured with the EIT/ERT technique (Wang *et al.*, 2005; Abdullah *et al.*, 2011; Gumery *et al.*, 2011; Hamood-ur-Rehman *et al.*, 2013). ERT/EIT has the requirement that the material conductivity is stable and in a measurable range.

Table 1. Typical measurement techniques for hydrodynamic parameters.

| Measurement Technique | Categories | | Hydrodynamic Parameters | Authors |
|---|---|---|---|---|
| | Global | Local | | |
| Bed expansion | × | | Overall gas holdup | Zhang et al. (2002), Luo and Al-Dahhan (2010) |
| Differential pressure drop | × | | Volume averaged gas holdup | Klein *et al*. (2003), van Baten *et al*. (2003), Wu *et al*. (2009) |
| Liquid solution tracer | × | | Liquid circulation velocity and average liquid velocity | Zhang *et al*. (2002), van Baten *et al*. (2003), Vial *et al*. (2002) |

| | | | | |
|---|---|---|---|---|
| Hot-film anemometry | | × | Instantaneous velocities and turbulence characteristics | Ali *et al*. (2011) |
| Digital imaging | | × | Gas holdup, bubble size and size distribution, and even bubble rise velocity | Vial *et al*. (2002), Liu *et al.* (2011a) |
| Probe techniques | | × | Gas holdup, bubble size and size distribution, rise velocity, etc. | Wu *et al.* (2009), Lo and Hwang, (2003), Deng *et al*. (2010) |
| Laser Doppler Velocimetry | | × | Velocity fields | Vial *et al*. (2002) |
| Computed tomography | | × | Local gas holdup and distribution | Luo and Al-Dahhan (2010). |
| Computer automated radioactive particle tracking | | × | Time-averaged flow fields, e.g. velocity, shear stress and turbulence | Luo and Al-Dahhan (2008) |
| Particle image velocimetry | | × | Full-field, detailed and instantaneous flow field, e.g. velocity, turbulence, and shear stress, etc. | Wu and Merchuk, (2003), Fujiwara *et al.* (2004), Lin and Chen (2005), Ge *et al.* (2014) |
| Electric resistance/impedance tomography | | × | Local gas holdup, gas holdup distribution, gas velocity, mixing efficiency and liquid circulation time | Wang *et al*. (2005), Abdullah *et al*. (2011), Gumery *et al*. (2011), Hamood-ur-Rehman *et al*. (2013) |

### 1.1.3 Numerical simulation

Computational fluid dynamics (CFD) simulation is a powerful numerical method to investigate and predict the hydrodynamics and mass transfer performance of multiphase reactors. The approach is much less time-, labor- and capital-intensive than experimental studies (Versteeg and Malalasekera, 1995). CFD simulation can provide extensive and

detailed data for systems that are difficult to investigate experimentally. CFD simulation allows in-depth analysis of fluid mechanisms in multiphase flow. However, CFD simulations can give confident and reliable predictions only when the used numerical models describe the physical phenomena properly and accurately. The need for accurate numerical models creates difficulties due to knowledge gaps and the complexity of fluid mechanics, especially with multiphase flow (Jacobsen *et al.*, 1997). Thus, rigorous experimental validation and verification of CFD simulations are still needed before the results can be considered reliable. Two-fluid models based on the Eulerian-Eulerian approach are commonly used for multiphase reactor simulations (Chen *et al.*, 2005; Tabib *et al.*, 2008; Šimčík *et al.*, 2011). In such two-fluid models, the continuous and dispersed phases are assumed to be interpenetrated and the momentum equations are described for each of the two phases in the Eulerian frame of reference. Turbulence sub-models and momentum transfer terms between the phases that describe the simulated case accurately are required to close the multiphase model.

Extensive numerical simulation studies of airlift reactors by CFD (Mudde and van den Akker, 2001; Huang *et al.*, 2007; Hekmat *et al.*, 2010; Huang *et al.*, 2010; Moraveji *et al.*, 2011; Šimčík *et al.*, 2011; Lestinsky *et al.*, 2015) have been reported and considerable progress has been achieved in the use of CFD approaches in ALR study. Huang *et al.* (2010) studied the applicability of gas-liquid mass transfer models for CFD simulation of an airlift reactor. Hekmat *et al.* (2010) and Lestinsky *et al.* (2015) investigated the effect of the draft tube on mixing and carried out optimization calculations for the bottom distance of the draft tube. Šimčík *et al.* (2011) performed CFD simulations of airlift reactors with air-water over three circulation flow regimes. They found that bubble circulations were not well captured in circulation flow regimes II and III.

Some researchers (Dhanasekharan *et al.*, 2005; Liu *et al.*, 2011a, b; Liu *et al.*, 2013; Amooghin *et al.*, 2015) have considered the effects of bubble size and adopted a population balance model (PBM) to account for bubble breakage and coalescence behaviour. Use of a PBM model is expected to improve modelling results since a two-fluid model with an assumption of a single bubble size can only give reasonable

predictions for cases where the bubbles have uniform size with negligible interactions. The PBM is able to describe the bubble size distribution (BSD) characteristics in multiphase flows when the kernels of bubble coalescence and breakup rates are provided as model closures. Dhanasekharan *et al.* (2005) used a discretized PBM in which bubble breakage and coalescence caused by turbulent eddies were taken into account to improve CFD simulation of gas holdup and mass transfer in an ALR with air-water. Liu *et al.* (2011a) developed a two-dimensional axisymmetric CFD model of a hairy root culture in an airlift bioreactor. In their developed model, a discretized PBM was utilized to describe the bubble size distribution and a porous media model was used to characterize the hairy root in the airlift bioreactor. With the developed model, Liu *et al.* (2011b) obtained satisfactory simulation results for mass transfer in the airlift bioreactor and optimized the reactor structure for hairy root culture (Liu *et al.* 2013). Amooghin *et al.* (2015) conducted simulations in which bubble breakup and coalescence were introduced by a two-group interfacial area transport equation to analyze the effects of the draft tube on hydrodynamics and mass transfer in airlift reactors. Three main bubble interactions were considered in the interfacial area transport equation: coalescence driven by turbulence, coalescence caused by wake entrainment, and breakup due to turbulent eddies.

## 1.2 Aim of the current research

This research focuses on airlift bioreactor hydrodynamics and mass transfer. Poor mass transfer of sparingly soluble gases is often considered as hindering commercialization of many novel green chemical and biochemical technologies utilizing airlift reactors (Munasinghe *et al*., 2015). The aim of the research was to achieve better understanding of mass transfer characteristics in airlift reactors through comprehensive experimental and numerical studies. Improved knowledge in this area can contribute to improved design and scale-up, and, potentially, lead to new industrial applications for airlift bioreactors. It is anticipated that the results obtained in this work using advanced measurement techniques will bring new insights into potential improvements to the mass transfer performance of airlift bioreactors.

**Effects of aeration modes**

The effects of the two aeration modes in airlift bioreactors – center-rising and annulus-ring – remain unclear for many airlift bioreactor applications, which makes it difficult to select the most suitable aeration mode in practical applications, especially with complex culture media. In the current research, the objective of investigating the effect of the aeration mode was to improve understanding of the pros and cons in order to be able to optimize aeration operation and facilitate practical bioreactor applications. Accurate results for local fluid flow structures and shear rate fields will provide researchers and engineers with valuable data and enable new thinking in airlift bioreactor design and optimization.

**Local gas holdup distribution and mass transfer performance**

Many chemical and biochemical processes operated in airlift reactors are limited by the mass transfer of sparingly soluble gaseous reactants, e.g. syngas (industrial tail gases) fermentation. Investigation of local gas holdup distribution, bubble size distribution and liquid-side mass transfer coefficients aims to develop understanding of the mass transfer characteristics and bring new insights for improvement of mass transfer in airlift bioreactors.

**Numerical model development and simulation**

In the current research, the aim of the numerical simulation study was to develop numerical models that are capable of performing reliable hydrodynamic simulation and providing accurate mass transfer predictions over homogenous and heterogeneous flow regimes and with non-Newtonian fluids. Such information is important since many bioprocesses are operated in the heterogeneous flow regime and with viscous non-Newtonian media.

## 1.3 Outline

This thesis comprises two main parts: a summary part and four publications in international scientific journals. The summary part has six sections: an introduction to the research background, a description of the experimental work, a description of

development of the numerical models, presentation of the results of the thesis work, presentation of the research conclusions, and suggestions for future work.

The research background is given in the introduction section, together with consideration of related literature on airlift reactors, typical measurement techniques and numerical simulation studies. The experimental design and measurement methods used in the current research are introduced in the experimental work section. The developed numerical models of the airlift bioreactor are briefly presented in the section on model development. Significant research results and corresponding analysis from Publications I – IV are presented in the results section. The conclusions of the current research and suggestions for future study are given in the last two sections of the summary part of the thesis.

## 1.4 Novel results

The following novel and interesting results were obtained in the current study.

i) In Publication I, it is found that the aeration mode has a remarkable effect on the liquid circulation structure in the airlift bioreactor. Liquid flow in the center-rising airlift bioreactor forms one large circulation cell throughout the reactor. In contrast, two counter-looping circulation structures of liquid flow exist in the annulus-rising airlift bioreactor. The two circulation cells in the annulus-rising airlift reactor increase the gas residence time and turbulence, and thereby enhance mass transfer efficiency.

ii) Visualized local gas holdup distributions were obtained, using a tomographic method, for an annulus-rising airlift reactor with non-Newtonian fluids commonly encountered in industry. The obtained gas holdup distributions are comparable to CFD simulation results in resolution and accuracy. The experimental results showed that the uniformity of gas distribution is significantly reduced by the viscosity of the liquid. This non-uniformity was slightly mitigated by an increase in superficial gas velocity. The local measurements bring new insights into feasible approaches for improving aeration and enhancing gas-liquid contact.

iii) A three-phase model (a liquid phase and two bubble phases) was developed for airlift bioreactors with low viscous Newtonian fluids. This model was able to produce reliable simulation results and give accurate predictions for airlift bioreactors over the three circulation regimes. The effect of reactor scale could be predicted reasonably well by the developed three-phase model at low computational cost.

iv) A computational fluid dynamic model for an airlift bioreactor with non-Newtonian fluids was developed that takes into account wide bubble size distribution and complex bubble coalescence and breakage mechanisms. Well-matched simulation results for overall gas holdup, bubble size and local flow structures demonstrated that the developed computational fluid dynamic model is able to describe and predict the hydrodynamics in airlift bioreactors with non-Newtonian fluids with reasonable accuracy.

# 2. Experimental work

The measurement methods employed in the current research work are described in this section. The measurement methods used included both advanced measuring techniques – particle image velocimetry, electrical impedance tomography and digital imaging, and conventional approaches – bed expansion, differential pressure drop and dynamic oxygen absorption. Additionally, the experimental design and setup is briefly introduced. Detailed descriptions of the measurement techniques and the experimental design and setup are provided in Publications I, II and IV.

## 2.1 Measurement methods

### 2.1.1 Particle image velocimetry

A particle image velocimetry (PIV) technique was used in Publication I to investigate the characteristics of the velocity fields, shear rate field, local flow structure and liquid circulation time in the airlift reactors. In Publication IV, a PIV technique was used to investigate the velocity field characteristics of both the gas and liquid phases in an airlift reactor with Newtonian and non-Newtonian fluids. The PIV measurement results were also used to validate and verify the developed CFD model of an airlift bioreactor.

The PIV measurement system (LaVision GmbH) used in the experiments consisted of a double-pulsed Nd Yag laser, two high resolution CCD cameras (1600 × 1200 pixels) and DaVis 8.3 software. For the cases where the gas and liquid velocity fields were measured simultaneously, two CCD cameras were used to record the bubbles and liquid, respectively. The liquid velocity field was traced by PMMA-RhB fluorescent particles with a diameter range from 20 to 50 µm. The software DaVis 8.3 was used to analyze the velocity fields and shear rate profiles. The PIV measurements for gas-liquid flow in the ALR were carried out with aeration rates lower than 12 L/min. This limit was used since further increase in the aeration rate made optical access to the liquid flow difficult, which resulted in low probability of detection of valid velocity vectors. As it is reported (Deen

et al., 2000; Deen et al., 2001), PIV technique is still limited to bubbly flows with low gas holdup, although it works well for single-phase flows.

### 2.1.2 Electrical impedance tomography

Electrical Resistance/Impedance Tomography (ERT/EIT) has been widely used to study gas-liquid mixing, volume fractions and their distributions, and fluid flow patterns for stirred tanks and bubble columns (Wang *et al*., 2005; Abdullah *et al*., 2011). In contrast, investigations on ALRs with ERT/EIT methods have only seldom been reported (Gumery *et al*., 2011; Hamood-ur-Rehman *et al*., 2013).

In Publication II, a three-dimensional EIT technique was used to extract local gas holdup data and to visualize the gas holdup distribution. An EIT system (Kuopio Impedance Tomography 4, KIT4) developed in the University of Eastern Finland (Kourunen *et al*., 2009) was used to investigate the effects of the liquid apparent viscosity and the aeration rate on the gas holdup and its distribution in an annulus-rising airlift bioreactor (Publication II). Three groups of 3-plane EIT sensors were installed to detect the conductivity distribution at three heights in order to obtain the gas holdup at typical axial positions in the airlift reactor. 48 sensors were equally distributed in three planes for each axial position. The designed EIT sensors layout and the EIT measuring procedure used are described in Publication II. Local, detailed and well-visualized results of the gas holdup distribution can give better understanding of the gas hydrodynamics and bring new insights into possible approaches to enhance gas-liquid mass transfer by improving the effectivity of gas-liquid contact.

### 2.1.3 Digital imaging

In the current research, a high-resolution CCD camera was used for digital imaging measurements based on the back-lighting method. To reduce the error caused by overlapping bubbles, an overlapping object recognition algorithm available from PORA software (Eloranta *et al.*, 2008) was used to identify the bubbles and analyze the bubble size distributions.

In Publication II, a digital imaging method was used to investigate the effect of liquid viscosity and aeration rate on the bubble size distribution. The bubble Sauter mean diameter was calculated and the interfacial area evaluated using measured gas holdup data. In Publication III, the gas phase was divided into small bubble and large bubble phases for CFD simulation. The number of gas bubble phases and the mean bubble size in each phase were determined based on the digital imaging measurements. In Publication IV, the bubble size and the corresponding volume fraction were estimated based on the digital imaging method.

### 2.1.4 Bed expansion and differential pressure drop methods

The bed expansion method was used to measure the overall gas holdup (Publications I - IV). The dependence of the overall gas holdup on the gas superficial velocity was used to characterize the flow pattern and for comparison with numerical simulation results. In Publication II, the differential pressure drop method was employed to examine the applicability of the three-dimensional EIT to airlift reactor measurement.

### 2.1.5 Dynamic oxygen absorption method

A dynamic oxygen absorption method was used to experimentally investigate the mass transfer performance of airlift reactors in Publications I – III. The method assumes that the liquid phase is mixed perfectly and that oxygen depletion from the gas bubbles is negligible.

## 2.2 Experimental systems and setups

### 2.2.1 Experimental systems

In Publication I, tap water and a solution of 0.0025 g/g Carboxyl Methyl Cellulose (CMC, Finnfix 50000), 6.6 g/L $(NH_4)_2SO_4$, and 3.7 g/L $KH_2PO_4$ were selected to mimic a low viscous medium in bioprocesses and cellulase enzyme cultivation solutions (Ahamed and Vermette, 2008), respectively.

In Publication II, CMC solutions of different mass concentrations were utilized to investigate the effect of non-Newtonian fluids on hydrodynamics and mass transfer. Tap water, as a Newtonian fluid, was used for comparison purposes.

In Publication IV, a solution with 0.14% mass fraction CMC was used as an example of a non-Newtonian fluid to investigate the developed numerical model of an airlift bioreactor.

The dynamic viscosity of the fluids used in the research work was measured with a modular compact rheometer (MCR 302, Anton Paar, Austria) at a shear rate range from 1 to 1000 1/s, as shown in Figure 2.

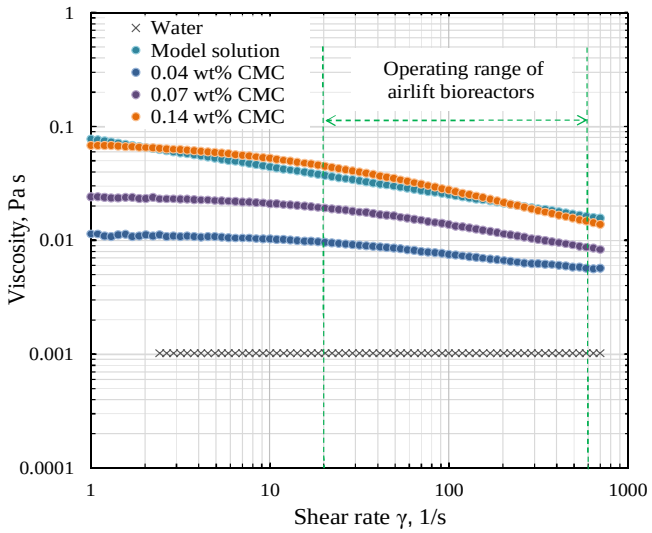


Figure 2. Liquid rheologies of the air-liquid systems.

The solutions used in the work exhibited shear thinning behavior and the apparent viscosity, $\mu_{app}$, can be described by the power law model. The consistency index $\kappa$ and the flow index $n$ of the fluids were estimated by fitting a power law equation with the least-squares method, as given in Table 2. The surface tension was measured using the pendant drop method with a contact angle and surface tension meter (CAM 100, KSV, Finland). The measured values are given in Table 2, together with other physical properties of the fluids.

**Table 2. Physical properties of the liquid phases used in the experiments, (Temperature: 20 °C).**

| Liquid phase | Density $kg \cdot m^{-3}$ | Surface Tension $N \cdot m^{-1}$ | Conductivity, $mS \cdot cm^{-1}$ | Apparent viscosity | | |
|---|---|---|---|---|---|---|
| | | | | $\kappa$ $Pa \cdot s^n$ | n | $\mu_{app}$ ($\gamma$= 50 $s^{-1}$) Pa·s |
| Tap water | 1000.2 | 0.071 | 0.109 | - | - | 0.0011 |
| Model solution | 1013.5 | 0.064 | - | 0.078 | 0.755 | 0.0316 ($\gamma$= 40 $s^{-1}$) |
| 0.04 wt% CMC | 1000.8 | - | 0.135 | 0.016 | 0.84 | 0.0086 |
| 0.07 wt% CMC | 1001.2 | - | 0.146 | 0.038 | 0.77 | 0.0164 |
| 0.14 wt% CMC | 1001.9 | - | 0.198 | 0.118 | 0.68 | 0.0351 |

### 2.2.2 Experimental setup and aeration modes

All experimental investigations were carried out in a laboratory-scale internal loop airlift bioreactor. Two aeration modes, gas feed into the draft tube (riser) – center-rising, and gas feed into the annulus (riser) between the draft tube and the outer column – annulus-rising, were operated and experimentally studied in Publication I. Schematic diagrams of the center-rising airlift bioreactor and the annulus-rising airlift bioreactor are shown in Figure 3 (a) – (b), respectively. The dimensions of the experimental setup and the operating conditions are given in detail in Publication I.

The annulus-rising airlift bioreactor was also used in the experimental and simulation investigations in Publications II - IV. To investigate the effect of the reactor scale, a large-scale annulus-rising airlift bioreactor with similar configuration was studied by simulation, as described in Publication III.

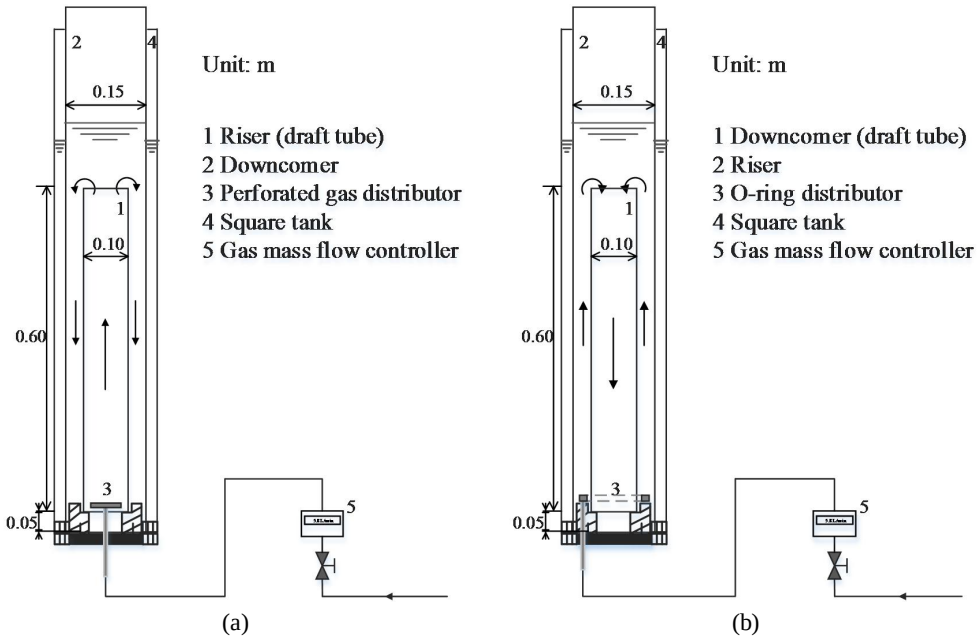


Figure 3. Schematic diagram of the experimental setup: (a) Center-rising airlift reactor (CR-ALR), (b) Annulus-rising airlift reactor (AR-ALR).

# 3. Development of numerical models for airlift reactors

A two-fluid model with an assumption of a single bubble size can give reasonable predictions for multiphase reactors where the bubbles have a narrow size distribution. However, in airlift reactors, simulations and predictions with a single bubble size are not usually satisfactory for circulation flow regimes II and III (Šimčík et al., 2011). Moreover, many chemical and biochemical processes are operated in heterogeneous flow, where bubble interactions might be pronounced and cause the bubble size distribution to be wide, particularly in fluids with complex physical properties. For this reason, numerical models capable of prediction for different circulation flow regimes (Publication III) and models able to describe the complex physical phenomena in airlift bioreactors (Publication IV) were developed.

## 3.1 Three-phase numerical model for airlift reactors

The three-phase model of an ALR (Publication III) includes two bubble phases as the dispersed phases and one liquid continuous phase. The two dispersed bubble phases are defined as the large bubble phase and the small bubble phase, respectively. For each bubble phase, the bubbles have a uniform size and different mean diameter value depending on the superficial gas velocity. In the investigated range of superficial gas velocity, the bubble size varies from 0.005 to 0.008 m for the large bubble phase and from 0.001 to 0.003 m for the small bubble phase in diameter (Publication III, Table II). The diameter ranges of the two bubble phases were determined based on experimental evaluation of bubble size in different sections of the airlift reactor. Momentum transfer between the two bubble phases is not considered, neither is bubble coalescence and breakage. The momentum transfer between the liquid phase and the bubble phases is formulated by taking the drag, lift, wall lubrication and turbulent dispersion forces into account (Publication III, Table III). The standard $k$ - $\varepsilon$ turbulence model was used to account for the liquid shear-induced turbulent viscosity. The bubble-induced turbulence

contribution was considered by adding an extra viscosity into the effective viscosity, where the extra viscosity was calculated using the Sato model (Sato et al., 1981).

The developed three-phase model (Publication III) improves the predictive capacity of the approach for the circulation flow regime III in ALRs and it is computationally economic compared with models involving a PBM. The three-phase model, which includes a mass transfer model based on penetration theory (Cockx *et al.*, 2001), is well capable of predicting the hydrodynamics and mass transfer of airlift reactors with low viscous fluids ($\mu_L$<0.005 Pa s) over the three circulation flow regimes. Furthermore, the effect of reactor scale on hydrodynamics and mass transfer is simulated and predicted reasonably well when compared with experimental results reported in literature.

## 3.2 Coupled CFD-PBM model for airlift bioreactors

### 3.2.1 The discrete PBM

A PBM can be considered as a transport equation for particle number density or its corresponding parameters. The PBM can describe and simulate bubble characteristics in gas-liquid flow when suitable bubble breakup and coalescence kernel models are used for its closure. In the absence of dissolution or evaporation, the discrete PBM for the volume fraction of bubble group *i* in gas holdup can be expressed as (Wang *et al.*, 2003; Xing *et al.*, 2013):

$$\frac{\partial}{\partial t}(\alpha_g f_i)+\nabla\cdot\left(\alpha_g \mathbf{u}_b f_i\right)= \sum_{\substack{j,k \\ x_{i-1}\le(x_j+x_k)\le x_{i+1}}}^{j\ge k}(1-\frac{1}{2}\delta_{j,k})\eta_{i,jk}c_{j,k}\alpha_g f_i\alpha_g f_k v_i/v_j/v_k - \alpha_g f_i\sum_{k=1}^{M}c_{i,j}\alpha_g f_k/v_k+\sum_{k=i}^{M}\psi_{i,k}\alpha_g f_k b_k v_i/v_k-\alpha_g b_i f_i \quad (1)$$

where $a_g$ is the gas holdup and $v_i$ is the bubble volume of bubble group *i*. $f_i$ is the volume fraction in gas holdup of bubble group *i*. $\eta_{i,k}$ is the distributing coefficient due to bubble coalescence and $\psi_{i,k}$ is the distributing coefficient related to bubble breakup. $c_{i,j}$ is the bubble coalescence rate and $b_i$ is the bubble breakup rate.

### 3.2.2 Bubble breakup mechanisms and kernel models

Bubble breakup mechanisms can be described by the balance between the external disruptive force and the sum of the interfacial tension force and viscous stress of fluid inside a bubble. Bubble breakup is determined by hydrodynamic conditions in the surrounding fluid and the characteristics of the bubble itself. The size of unstable bubbles that start to deform and possibly split into two or more daughter bubbles can be evaluated from this force balance (Hinze, 1955; Acrivos, 1983). Generally, four mechanisms for bubble breakup are categorized as: 1) turbulence fluctuations and eddy collisions; 2) viscous shear stress; 3) the shearing-off process; and 4) interfacial instability (Liao and Lucas, 2009). Compared with bubble breakup induced by turbulence fluctuations and eddy collisions, studies on the theory and modelling of bubble breakup caused by viscous shear, shearing-off and surface instability are rather rare.

In turbulent flow, bubble breakup is mainly caused by turbulence fluctuations or by turbulent eddies. A variety of kernel models have been developed for bubble breakup rate formulation based on different breakup criteria in terms of critical turbulent kinetic energy (Chatzi *et al.*, 1989; Luo and Svendsen, 1996; Prince and Blanch, 1990), critical inertial force (Lehr and Mewes, 2001; Lehr *et al.*, 2002), critical velocity fluctuation (Alopaeus *et al.*, 2002), and the combination of critical turbulent kinetic energy and inertial force (Wang *et al.*, 2003; Zhao and Ge, 2007). Typical bubble breakup kernel models are given in Table 3.

For bubbles experiencing significant viscous shear stress in the continuous phase, the interfacial tension force is not able to maintain the bubble shape and the bubble ruptures into two almost equal size daughters or several small bubbles. Shear stress can result from a large velocity gradient of fluid around the bubble. Shear stress across a bubble wake region, where a large part of the trailing bubble is outside the wake, may also lead to bubble breakup. The critical diameter for bubble breakup can be evaluated based on a critical capillary number that depends on the viscosity ratio and the flow type (Grace, 1982). In simple shear flow, the breakup frequency for bubbles larger than the critical

Table 3. Typical kernel models for bubble breakup caused by turbulent eddies.

| Author | Equation |
|---|---|
| Prince & Blanch (1990) | $b(d)=\int_{0.2d}^{l}\frac{0.07\pi^4}{\lambda^4}(d+\lambda)^2(d^{2/3}+\lambda^{2/3})^{1/2}\varepsilon^{1/3}\exp\left(-\frac{1.18}{\lambda^{2/3}}\frac{\sigma}{\rho_l d\varepsilon^{2/3}}\right)d\lambda$ |
| Luo & Svendsen (1996) | $b(d)=\int_0^{0.5}b\left(f_v\middle\|d\right)\mathrm{d}f_v,\quad b(f_v\|d)=0.923(1-\alpha_g)n(\frac{\varepsilon}{d^2})^{1/3}\int_{\xi_{\min}}^{1}\frac{1+\xi^2}{\xi^{11/3}}\exp\left(-\frac{12c_f\sigma}{\beta\rho_l\varepsilon^{2/3}d^{5/3}\xi^{11/3}}\right)d\xi$ |
| Lehr (2002) | $b(d)=\int_0^{0.5}b\left(f_v\middle\|d\right)\mathrm{d}f_v,\quad b(f_v\|d)=\int_{d_1}^{d}0.8413\sqrt{2}\frac{\sigma}{\rho_l\varepsilon^{2/3}d_1^4}\frac{(\lambda+d)^2}{\lambda^{13/3}}\exp\left(-\frac{2\sigma}{\rho_l\varepsilon^{2/3}d_1\lambda^{3/2}}\right)d\lambda$ |
| Wang (2003) | $b(d)=\int_0^{0.5}b\left(f_v\middle\|d\right)\mathrm{d}f_v,$<br>$b(f_v\|d)=0.923(1-\alpha_g)\varepsilon^{1/3}\int_{\lambda_{\min}}^{\lambda}P_b\left(f_v\middle\|d,\lambda\right)(\lambda+d)^2\lambda^{-11/3}d\lambda$<br>$P_b\left(f_v\middle\|d,\lambda\right)=\int_0^{\infty}P_b\left(f_v\middle\|d,e(\lambda),\lambda\right)P_e\left(e(\lambda)\right)\mathrm{d}e(\lambda),\quad P_e\left(e(\lambda)\right)=1/\bar{e}(\lambda)\exp\left(-e(\lambda)/\bar{e}(\lambda)\right)$<br>$\bar{e}(\lambda)=\frac{\pi}{6}\lambda^3\rho_l\frac{\overline{u}_\lambda^2}{2},\quad P_b\left(f_v\middle\|d,e(\lambda),\lambda\right)=\begin{cases}1/(f_{v,\max}-f_{v,\min}) & f_{v,\max}-f_{v,\min}\geq\delta\ \&\ f_{v,\min}<f_v<f_{v,\max}\\ 0 & \text{else}\end{cases}$<br>$c_{f,\max}=\min\left((2^{1/3}-1),e(\lambda)/(\pi d^2\sigma)\right),\quad f_{v,\min}=\left(\pi\lambda^3\sigma/(6e(\lambda)d)\right)^3$<br>$b_{bi}(d)=b^*\frac{(d-d_c)^m}{(d-d_c)^m+d_c^m}$ |

size can be calculated using empirical correlations (Elemans *et al.*, 1993).

In the shearing-off process, a large bubble usually fragments into a number of small daughter bubbles, and the breakup mechanism is complicated and difficult to describe (Fu and Ishii, 2002). In highly viscous flows, bubble skirt becomes unsteady and shears off into a number of small bubbles at the rim when the relative velocity between the bubble and the liquid phase is high enough. However, experimental and theoretical investigations have shown that the interfacial viscous shear force in air-water flow or low viscous systems can be negligible (Liao and Lucas, 2009).

Bubble breakup due to instability occurs when the bubble volume is larger than a maximum stable limit. Depending on the density ratio, instabilities are classified as Rayleigh-Taylor and the Kelvin-Helmholtz instability. Rayleigh-Taylor instability appears when a light fluid is accelerated in a heavy fluid. Kelvin-Helmholtz instability is dominant in a breakup process when the densities of the two phases are close to each other. The bubble breakup frequency due to instability can be formulated using empirical correlations (Wang *et al.*, 2005a, b).

To solve the PBM, two bubble breakup mechanisms – turbulent eddy collisions and interfacial instability, were considered in this study (Publication IV) based on the hydrodynamic characteristics investigated in the ALR and the bubble breakup kernel models themselves. In general, the bulk shear stress field in ALRs is mild compared to mechanically stirred tanks or bubble columns (Chisti, 1989), particularly at low and medium aeration rates. In the experimental study of Publication I, a uniform and low-strength bulk shear rate field was obtained in the ALR under the investigated conditions (Figure 7 in Publication I). The turbulence level is significant only at the sparger region and at the inlet and outlet zones of the draft tube, due to the combined effects of the sudden enlarged cross-section, reversed liquid flow direction, deformed bubbles, and intensive bubble movements and interactions. Turbulence fluctuations and eddy collisions is considered in many studies (Dhanasekharan *et al.*, 2005; Liao and Lucas, 2009; Liu *et al.*, 2011a, b; Liu *et al.*, 2013) as the dominant bubble breakup mechanism in turbulent flows, which is the most common case in chemical, petrochemical, biochemical and

environmental processes. The kernel models for bubble breakup caused by turbulence have been widely studied and are relatively well understood, and they are easy to use to close the PBM (Liao and Lucas, 2009). Bubble breakup due to interfacial instability is included in the developed model and used to describe the phenomenon where large bubbles are formed in a viscous liquid medium and cannot survive due to their instability.

The bubble breakup rate caused by turbulent eddies was calculated using the kernel model proposed by Wang *et al.* (2003), given in Table 4 (Table II of Publication IV). In the Wang's model, two criteria - turbulent kinetic energy of the hitting eddy greater than a critical value, and inertial force of the hitting eddy greater than the interfacial force of the smallest daughter, are taken into account to calculate the bubble breakup. Figure 4 illustrates the effect of the energy dissipation rate $\varepsilon$ on the breakup rate of mother bubbles of size $d_b$ for typical $\varepsilon$ values in ALRs under the operating conditions used in the study.

Table 4. Bubble breakup and coalescence kernel models used in the study.

| Mechanism | Equation |
|---|---|
| Bubble breakup due to turbulent eddies | $\mathrm{b}(d)=\int_0^{0.5} b\left(f_v\middle\vert d\right)\mathrm{d}f_v$<br>$b(f_v\vert d)=0.923(1-\alpha_g)n\varepsilon^{1/3}\int_{\lambda_{\min}}^{d_b} P_b\left(f_v\middle\vert d,\lambda\right)(\lambda+d)^2\lambda^{-11/3}d\lambda$<br>$P_b\left(f_v\middle\vert d,\lambda\right)=\int_0^{\infty} P_b\left(f_v\middle\vert d,e(\lambda),\lambda\right)P_e\left(e(\lambda)\right)\mathrm{d}e(\lambda),\ P_e\left(e(\lambda)\right)=(1/\bar{e}(\lambda))\exp\left(-e(\lambda)/\bar{e}(\lambda)\right)$<br>$P_b\left(f_v\middle\vert d,e(\lambda),\lambda\right)=\begin{cases}1/(f_{v,\max}-f_{v,\min}) & f_{v,\max}-f_{v,\min}\geq\theta\ \&\ f_{v,\min}<f_v<f_{v,\max}\\ 0 & \text{else}\end{cases}$<br>$f_{v,\min}=\left(\pi\lambda^3\sigma/(6e(\lambda)d)\right)^3,\ (f_{v,max}^{2/3}+(1-f_{v,max})^{2/3}-1)=\min\left((2^{1/3}-1),e(\lambda)/(\pi d^2\sigma)\right),\bar{e}(\lambda)=\frac{\pi}{6}\lambda^3\rho_l\frac{\bar{u}_\lambda^2}{2}$ |
| Bubble breakup due to interfacial instability | $b_{in}(d)=b^*\dfrac{(d-d_c)^m}{(d-d_c)^m+d_c^m},\quad \beta\left(f_v,d\right)=2\delta(0.5)$ |
| Bubble coalescence due to turbulent eddies | $c_T(d_i,d_j)=\omega_T(d_i,d_j)P_T(d_i,d_j)$<br>$\omega_T(d_i,d_j)=(\pi/4)\alpha_{\max}(\alpha_{\max}-\alpha)^{-1}\Gamma_{ij}\sqrt{2}\varepsilon^{1/3}(d_i+d_j)^2(d_i^{2/3}+d_j^{2/3})^{1/2}$<br>$P_T(d_i,d_j)=\exp\left(-\left(0.75(1+\xi_{ij}^2)(1+\xi_{ij}^3)\right)^{1/2}(\rho_g/\rho_l+\gamma)^{-1}(1+\xi_{ij})^{-3}We_{ij}^{1/2}\right)$<br>$\Gamma_{ij}=l_{bt,ij}^m/(l_{bt,ij}^m+h_{b,ij}^m),l_{bt,ij}=\left(l_{bt,i}^2+l_{bt,j}^2\right)^{1/2},l_{bt}=0.89d_b,h_{b,ij}=\left(N_i+N_j\right)^{1/3}$ |

| | |
|---|---|
| Bubble coalescence due to wake entrainment | $c_W(d_i,d_j)=\omega_W(d_i,d_j)P_W(d_i,d_j)$<br>$\omega_W(d_i,d_j)=12.0\Theta d_i^2\bar{u}_{slip,i},\quad \bar{u}_{slip,i}=0.71\sqrt{gd_i}$<br>$P_W(d_i,d_j)=\exp(-0.46\rho_l^{1/2}\varepsilon^{1/3}\sigma^{-1/2}(d_i d_j/(d_i+d_j))^{5/6})$<br>$\Theta=\begin{cases}\left(d_j-d_{cw}/2\right)^6\Big/\left(\left(d_j-d_{cw}/2\right)^6+\left(d_{cw}/2\right)^6\right) & d_j\geq d_{cw}/2\\ 0 & else\end{cases}$ |
| Bubble coalescence due to different rise velocities | $c_U(d_i,d_j)=\omega_U(d_i,d_j)P_U(d_i,d_j)$<br>$\omega_U(d_i,d_j)=\pi/4(d_i+d_j)^2\left\lvert u_{ri}-u_{rj}\right\rvert,$<br>$P_U(d_i,d_j)=0.5$ |

The bubble breakup rate increases with increase in the energy dissipation rate, which increases the bubble-eddy collision frequency and the kinetic energy contained in eddies. The increase of mother bubble size increases the number of eddies with a size equal to or smaller than the bubble and results in increasing bubble-eddy collision frequency and thereby increasing bubble breakup rate. The effect of liquid viscosity on the bubble breakup rate can be reasonably predicted, as shown in Figure 5. The effect of viscosity on the breakup rate is not significant when the value of the viscosity is low. With increasing viscosity (> 0.01 Pa s) the breakup rate decreases significantly, especially for small bubbles. This prediction is in accordance with both experimental study (Wilkinson *et al.*, 1993) and physical theory. The number of eddies with a size equal to or smaller than the bubble decreases with increasing viscosity, which results in decreasing collision

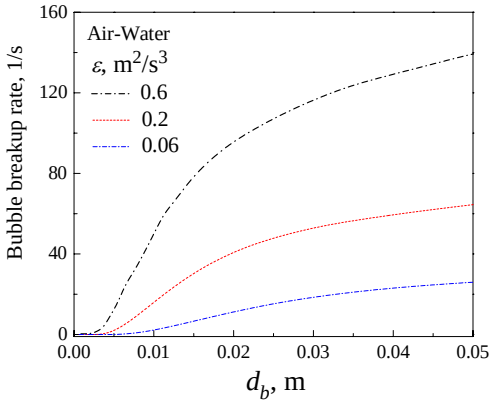


Figure 4. Effect of energy dissipation rate on the bubble breakup rate.

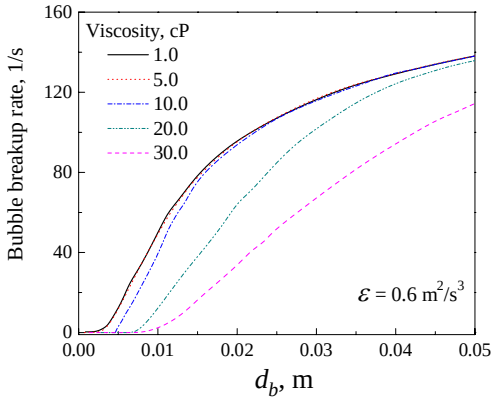


Figure 5. Effect of viscosity on the bubble breakup rate.

frequency and therefore decreasing breakup rate. The bubble breakup due to instability was formulated using the kernel model from Wang *et al.* (2005a, b) given in Table 4. This breakup mechanism only affects the volume fraction of large bubbles.

### 3.2.3 Bubble coalescence mechanisms and kernel models

Bubble coalescence results from the interaction of bubbles with the surrounding fluid and interactions between approaching bubbles. Three theories have been presented to describe the bubble coalescence process: the film drainage model (Shinar and Church, 1960), the energy model (Howarth, 1964), and the critical approach velocity model (Lehr and Mewes, 2001; Lehr *et al.*, 2002). The bubble coalescence rate includes the coalescence frequency, which is determined by the bubble collision mechanism, and the coalescence efficiency, whose formulation depends on the coalescence theory used. The most popular and widely used coalescence mechanism model is the film drainage model where the bubble coalescence efficiency is characterized by the contact time and the drainage time (Liao and Lucas, 2010). A variety of physical models characterized by the collision mechanism are available to calculate bubble coalescence frequency in a turbulent flow. Based on the collision mechanism, kernel models for bubble coalescence frequency can usually be classified into: 1) turbulent fluctuations in the surrounding fluid; 2) mean velocity gradient in the flow; 3) different bubble rise velocities; 4) bubble capture in an eddy; and 5) wake interactions (Liao and Lucas, 2010). Typical kernel models of bubble coalescence frequency and efficiency available in the literature are given in Table 5, where $c(d_i, d_j)$ is given without the number density of bubbles $i$ and $j$. To solve the PBM, the number density of the bubbles needs to be included, as given in Equation (1).

Based on the investigated hydrodynamic characteristics in the ALR, the cumulative contribution from three bubble coalescence mechanisms were included in the study (Publication IV) together with two bubble breakup mechanisms. The three coalescence mechanisms are bubble coalescence due to turbulent eddies ($c_T$), coalescence due to different bubble rise velocities ($c_U$) and coalescence due to wake entrainment ($c_W$). The kernel models proposed by Wang *et al.* (2005a, b) were used in the study (Publication IV), given in Table 4. In the kernel model for bubble breakup due to turbulent eddies, the

Table 5. Typical kernel models for bubble coalescence frequency and efficiency in turbulent flows.

| Author | Equation | | |
|---|---|---|---|
| | Coalescence rate | Collision frequency | Coalescence efficiency |
| Prince & Blanch (1990) | $c(d_i,d_j)=(\omega_T+\omega_U+\omega_S)P_C$ | $\omega_T = 0.089\pi\varepsilon^{1/3}(d_i+d_j)^2(d_i^{2/3}+d_j^{2/3})^{1/2}$<br>$\omega_U = 0.25\pi d_i+d_j)^2\left\|u_{bi}-u_{bj}\right\|$<br>$\omega_S = 1/6(d_i+d_j)^3(dU_c/dR)$ | $P_c = \exp\left(-\frac{r_{ij}^{5/6}\rho_l^{1/2}\varepsilon^{1/3}}{4\sigma^{1/2}\varepsilon^{1/3}}\ln\frac{h_0}{h_f}\right)$ |
| Luo & Svendsen (1996) | $c(d_i,d_j)=\omega_T P_C$ | $\omega_T = \frac{\pi}{4}\sqrt{2}\varepsilon^{1/3}(d_i+d_j)^2(d_i^{2/3}+d_j^{2/3})^{1/2}$ | $P_C = \exp\left(-c_e\frac{\left(0.75(1+\xi_{ij}^2)(1+\xi_{ij}^3)\right)^{1/2}}{(\rho_g/\rho_l+\gamma)(1+\xi_{ij})^3}We_{ij}^{1/2}\right)$ |
| Lehr (2002) | $c(d_i,d_j)=\frac{\pi}{4}\left(d_i+d_j\right)^2\min(u',u_{crit})\exp\left(-(\alpha_{\max}^{1/3}/\alpha^{1/3}-1)^2\right)$<br>$u'=\max\left(\sqrt{2}\varepsilon^{1/3}\sqrt{d_i^{2/3}+d_j^{2/3}},\left\|\mathbf{u}_{bi}-\mathbf{u}_{bj}\right\|\right)$ | | |
| Wang et al. (2005a, b) | $c(d_i,d_j)=\omega_I P_T+\omega_W P_W+\omega_U P_U$ | $\omega_T = \frac{\pi}{4}\frac{\alpha_{\max}}{\alpha_{\max}-\alpha}\Gamma_{ij}\sqrt{2}\varepsilon^{1/3}(d_i+d_j)^2(d_i^{2/3}+d_j^{2/3})^{1/2}$<br>$\omega_W = 12.0\Theta d_i^2\bar{u}_{slip,i}$<br>$\omega_U = \pi/4(d_i+d_j)^2\left\|u_{ri}-u_{rj}\right\|$ | $P_T = \exp(\frac{-\left(0.75(1+\xi_{ij}^2)(1+\xi_{ij}^3)\right)^{1/2}}{(\rho_g/\rho_l+\gamma)(1+\xi_{ij})^3}We_{ij}^{1/2})$<br>$P_W = \exp(\frac{-0.46\rho_l^{1/2}\varepsilon^{1/3}}{\sigma^{-1/2}}(d_i d_j/(d_i+d_j))^{5/6})$<br>$P_U = 0.5$ |
| Bhole (2008) | $c(d_i,d_j)=\omega_T P_C$ | $\omega_T = \frac{\pi}{4}\sqrt{2}\varepsilon^{1/3}(d_i+d_j)^2(\frac{d_i^{2/3}}{1+S_{ti}}+\frac{d_j^{2/3}}{1+1+S_{tj}})^{1/2}$<br>$S_{ti} = \frac{\tau_{bi}}{\tau_f} = \frac{4C_V d_{bi}}{3C_D V_{bi}}/(C_\mu^{3/4}\frac{k}{\varepsilon})$ | $P_C = \exp\left(-\frac{r_{ij}^{5/6}\rho_l^{1/2}\varepsilon^{1/3}}{4\sigma^{1/2}\varepsilon^{1/3}}\ln\frac{h_0}{h_f}\right)$ |

effects of gas holdup and effective bubble turbulent path length is considered to modify the bubble collision frequency formulation. The contributions of the different bubble coalescence mechanisms are compared in Figure 6 in terms of bubble coalescence rate. It can be seen that $c_T$ is much larger than $c_W$ and $c_U$ when the bubble size is smaller than 10 mm. For large bubbles, $c_W$ and $c_U$ are dominant. $c_W$ increases rapidly with increasing bubble size, which implies that $c_W$ plays a crucial role in the non-homogeneous regime.

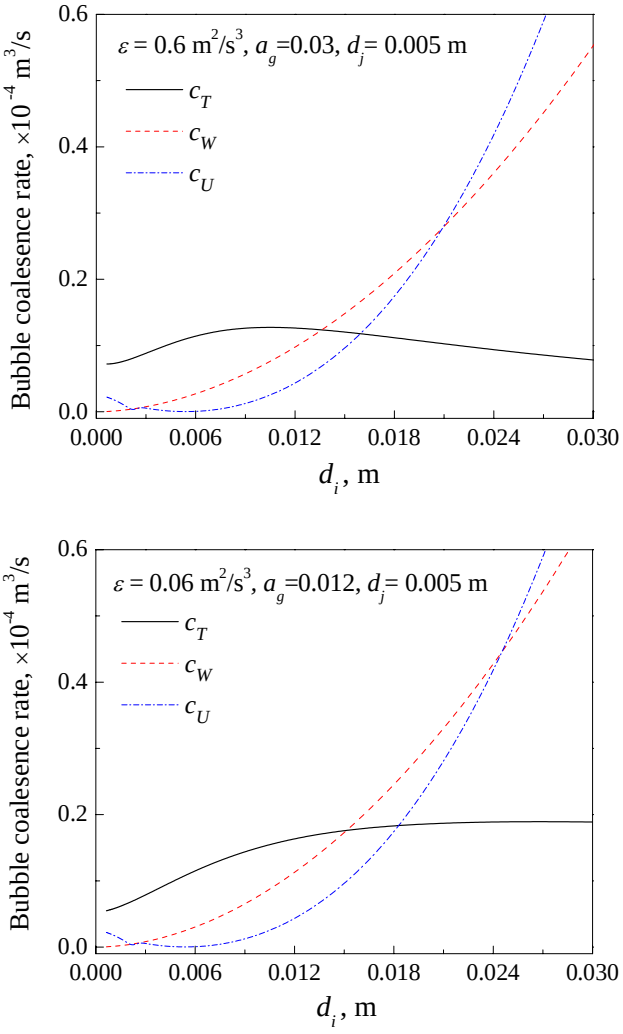


Figure 6. Bubble coalescence rate for different coalescence mechanisms.

Figure 7 shows the effect of viscosity on $c_U$ which increases with increasing viscosity. The effect of viscosity is limited to a certain range where bubble size is smaller than 5 mm. For large bubbles, $c_U$ is more sensitive to high viscosity. With the coalescence model used in this study, the viscosity has no effect on $c_T$ and $c_W$.

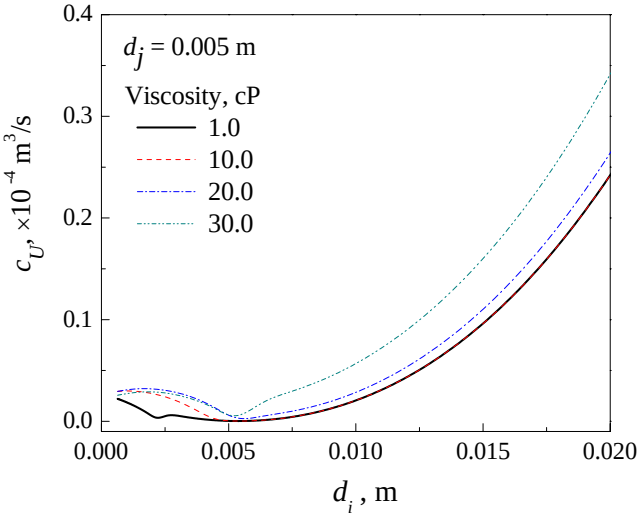


Figure 7. Effect of viscosity on the coalescence rate due to difference in bubble rise velocities.

3.2.4 Turbulence modelling for gas-liquid flows simulation

Turbulence in dispersed gas-liquid multiphase flow plays an important role in determining gas holdup distribution, liquid velocity fields, and mass and heat transfer. Turbulence in gas-liquid turbulent flow includes the shear-induced turbulence of the continuous phase and bubble-induced turbulence of the dispersed phase. The shear-induced turbulence of the continuous phase can be calculated using single-phase turbulence models. For dispersed gas-liquid turbulent flow in ALRs, the standard $k$-$\varepsilon$ turbulence model has been widely used, and it is considered a robust model with satisfactory accuracy (Lopez de Bertodano *et al.*, 1994; Lehr and Mewes, 2001; Wang *et al.*, 2005a, b; Xiang *et al.*, 2013). The presence of a gas phase in a liquid turbulent flow has effects on the structure and intensity of the turbulent motions. Turbulence can be generated by bubbles even in laminar flows, which is usually referred to as pseudo-

turbulence (Hosokawa and Tomiyama, 2013; Rzehak and Krepper, 2013 a, b). The introduction of bubble-induced turbulence is considered to be consistent with the physics of vertical bubbly flow and is important in gas-liquid multiphase flow, particularly for bubble breakup and coalescence processes.

For Eulerian two-fluid models based on a Reynolds averaged Navier Stokes approach, the bubble-induced turbulence can be simply included by adding an extra bubble-induced contribution to the effective viscosity, typically using the model proposed by Sato (1981). Satisfactory predictions for gas holdup and liquid velocity have been obtained (Rzehak and Krepper, 2013 a, b) using this approach to include the contribution of bubble-induced turbulence. The approach, however, does not predict directly turbulent kinetic energy or dissipation. In more complex approaches, the bubble-induced contribution is introduced by two-time constant models assuming superposition of turbulence models (Lahey *et al.*, 1993; Lopez de Bertodano *et al.*, 1994; Wang *et al.*, 2005 a, b; Xing et al., 2013) or by including source terms in the unmodified turbulence transport equations (Politano *et al.*, 2003; Rzehak and Krepper, 2013 a, b). The two-time constant equation modelling approach provides more accurate and improved prediction of turbulence kinetic energy and energy dissipation rate, and, in most cases, is preferable to the approach of simply adding an extra viscosity term.

In Publication IV of this thesis, bubble-induced turbulence was considered using the two-time constant model given in Table I of Publication IV (Lahey *et al.*, 1993). The two-time constant model is based on linear superposition of the shear-induced turbulence and the bubble-induced turbulence. Figure 8 illustrates the contribution of the bubble-induced turbulence calculated using the two-time constant model by comparing the calculated bubble-induced turbulence to the calculated shear-induced turbulence and the overall turbulence. In Figure 8, the radial profile of turbulent kinetic energy is compared for the air-CMC system at the top of the ALR with the PIV measurements carried out in this study. It can be seen that the contribution of the bubble-induced turbulence calculated using the two-time constant model is less than that of the shear-induced turbulence. However, taking the bubble-induced turbulence into consideration improves the

prediction of the turbulent kinetic energy relative to experimental data due to the increased turbulence generated by the flowing bubbles. Therefore, it is concluded that the two-constant model is suitable for modification of turbulence calculation for prediction of bubbly flow in ALRs.

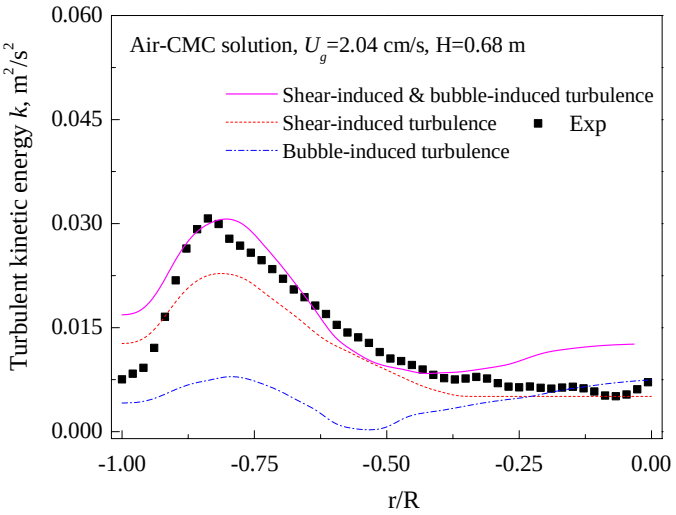


Figure 8. Comparison of turbulent kinetic energy between the simulation and experiment for air-CMC solution.

### 3.2.5 Coupling of PBM into CFD simulation

A computational fluid dynamics model coupled with a discretized population balance equation (Wang *et al.*, 2005b) was developed in Publication IV to simulate and predict hydrodynamics of airlift bioreactor. Multiple coalescence and breakage mechanisms (Publication IV, Table 2) were considered to account for the complex bubble interactions in non-Newtonian fluids, particularly in the heterogeneous flow regime. The multiple coalescence mechanisms included coalescence due to turbulent eddies, coalescence due to wake entrainment, and coalescence due to different rise velocities of bubbles. Bubble breakage caused by eddy collisions and large bubble instability (Wang *et al.*, 2005b; Xing *et al.*, 2013) were taken into account in the population balance equation. The bubble size was divided into 30 groups by the geometric method ($v_{i+1}=v_i q$), where the smallest bubble volume $v_1$ was $1.0\times10^{-10}$ m$^3$ and the factor $q$ was 1.7 (Wang *et al.*, 2005b). All the bubble

groups were assumed to have identical flow velocity. The drag, lift, wall lubrication and turbulent dispersion forces were considered in the momentum transfer between the gas and liquid phases in the momentum equations, where each bubble size class is used with the corresponding volume fraction to formulate the drag, lift, and wall lubrication forces (Publication IV, Table 1). A modified $k$-$\varepsilon$ model (Lahey *et al.*, 1993), which accounts for both the shear-induced turbulence and the bubble-induced turbulence, was used to describe the liquid phase turbulence. The turbulent viscosity of the gas phase was formulated based on the liquid turbulent viscosity (Jakobsen, 1993).

The coupling of the discretized population balance equation with the computational fluid dynamics model was implemented in ANSYS Fluent 14.5 by defining user-defined scalars. The volume fraction of the bubble group $i$ in the total gas volume was defined as a resolved scalar and resolved from its transportation equation in the solver. The bubble coalescence and breakage rates were introduced into the transportation equation using user-defined functions. The apparent viscosity of the non-Newtonian fluid was described with a power law equation (Publication IV, Eq. (1)) obtained from experiments. Bubble size distribution was resolved from the PBM using the gas holdup and the kinetic energy dissipation rate calculated in the CFD. The bubble size distribution obtained from the PBM was used to formulate the interphase forces and the turbulence modification closure terms for the two-fluid model.

# 4. Results and discussion

## 4.1 Experimental results

### 4.1.1 Effect of aeration modes

A detailed quantitative experimental investigation (Publication I) of the hydrodynamics and mass transfer was performed for the center- (CR-ALR) and annulus-rising airlift bioreactors (AR-ALR) to better understand the pros and cons of the aeration modes. Comparisons of the overall gas holdup, local liquid velocity, liquid circulation time, shear rate distribution and volumetric mass transfer coefficient were presented in order to facilitate selection of the aeration mode for internal-loop airlift bioreactor applications. The experimental results show that the overall gas holdup (Publication I, Fig. 3) is higher, for comparable conditions, in the AR-ALR than in the CR-ALR because more bubbles are entrained into the downcomer. This is in accordance with the better anti-foaming characteristics of the AR-ALR observed in the experiments (Publication I, Fig. 2). The increased liquid circulation time (Publication I, Fig. 6) in the AR-ALR compared with the CR-ALR indicates that the driving force for liquid circulation is lower due to increased gas holdup in the downcomer. The results suggest that there is a trade-off for ALRs between the two aeration modes regarding high gas holdup and fast mixing. Gas-liquid mass transfer performance in the AR-ALR is better than in the CR-ALR (Publication I, Fig. 9) in terms of $k_La$, although the effect of the aeration mode on $k_La$ is not as obvious as on the overall gas holdup.

Liquid velocity fields in the CR-ALR and AR-ALR were obtained for water and model solution from PIV measurements. As an example, Figure 9 (Publication I, Fig. 4) shows the liquid velocity fields for water and model solution in the CR-ALR and AR-ALR at $U_g$ 1.18 cm/s. For comparable conditions (Figure 9a versus Figure 9c and Figure 9b versus Figure 9d), the liquid velocity profiles are less uniform in the CR-ALR than in the AR-ALR, particularly for the air-model solution system. At the downcomer inlet location marked with a green dashed line in Figure 9, the local liquid circulating velocity into the

downcomer is higher in the AR-ALR than in the CR-ALR, which reasonably explains the higher overall gas holdup and the more extensive entrainment of bubbles in the AR-ALR. It can be noted that the flow structure at the top region of the CR-ALR clearly differs from that of the AR-ALR, as can be seen from Figure 9 (a) vs (c) and Figure 9 (b) vs (d). The liquid flow forms a large circulation cell in the CR-ALR, whereas two circulation cells exist in the AR-ALR due to a small cell appearing at the top region.

The shear fields of the CR-ALR and the AR-ALR at $U_g$ 1.18 cm/s are compared in Figure 10. It can be seen that the shear rate for the air-model solution is relatively high in the riser and downcomer of the CR-ALR compared to the air-water system. In the AR-ALR, the profile of the shear rate is little affected by the model solution and the shear rate becomes only slightly larger in the riser. This indicates that the homogeneity of the model solution is better in the AR-ALR than in the CR-ALR. In principle, this homogeneous environment, where the nutrient concentration gradient is lower, will benefit biomass cultivation processes. It is also found that the local maximum shear rate for the air-water system first increases and then decreases with increasing $U_g$. Therefore, increasing $U_g$ might be a way to improve the homogeneity of reaction media in fermentation processes operated in ALRs.

### 4.1.2 Local gas distribution and mass transfer characteristics

Superior performance of the AR-ALR over the CR-ALR as regards anti-foaming, high overall gas holdup, uniform shear rate fields and high overall mass transfer was found for bioprocess applications in Publication I. It was further noted that studies on AR-ALRs are relatively scarce compared to work on CR-ALRs (Koide *et al.*, 1983).

The mass transfer rate of sparingly soluble gas to the liquid phase is the limiting factor for many chemical and biochemical processes operated in ALRs and it often determines the achievable production yield. Additionally, aeration conditions selected based on bench-scale cultivation studies may not generate sufficiently effective gas distribution in airlift bioreactors, which might lower the specific mass transfer rate and the expected yield of desired products (Lennartsson *et al.*, 2011). Therefore, extensive experimental

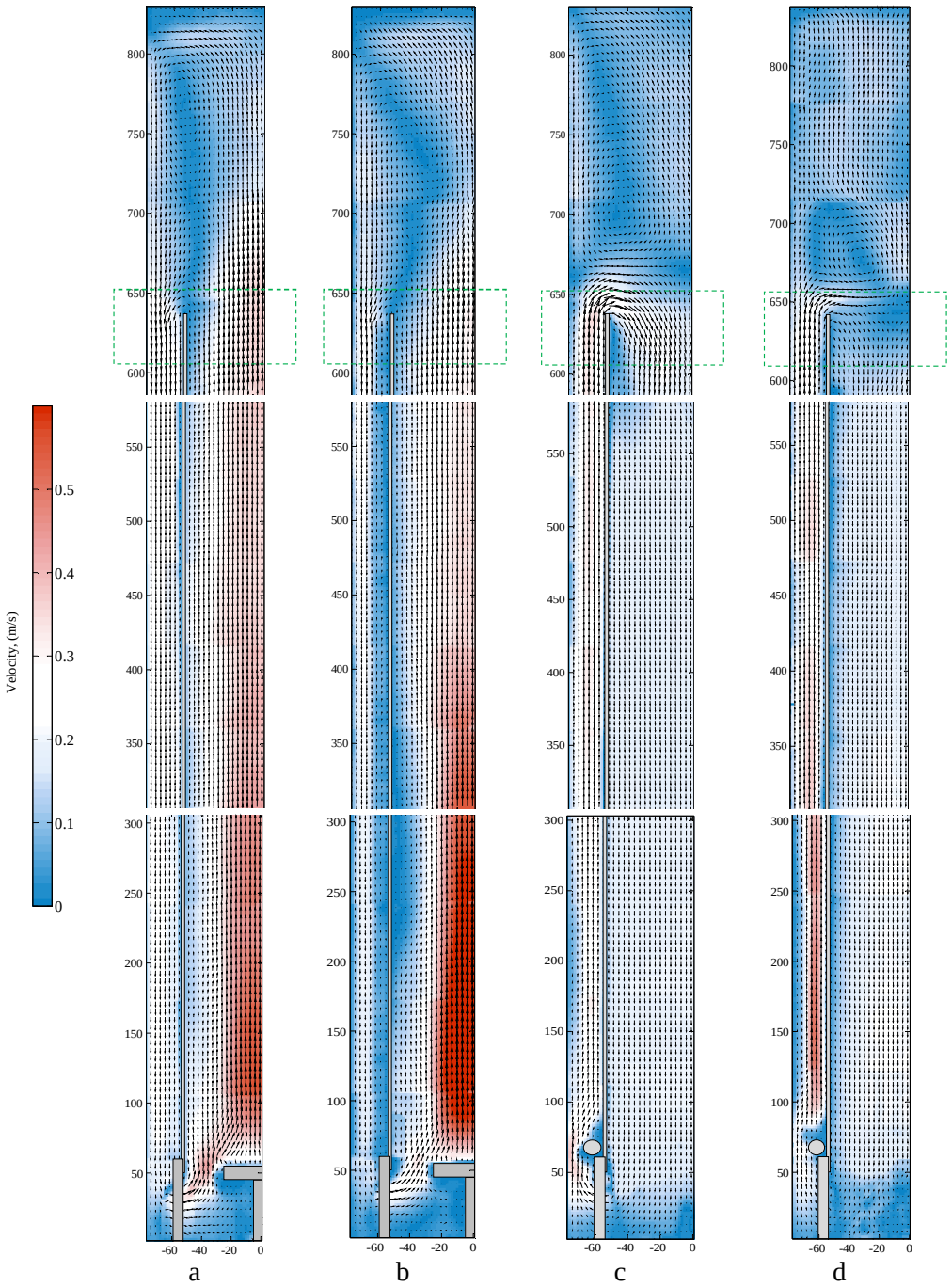


Figure 9. Liquid velocity fields at $U_g$ 1.18 cm/s: (a) CR-water, (b) CR- model solution, (c) AR- water, (d) AR- model solution.

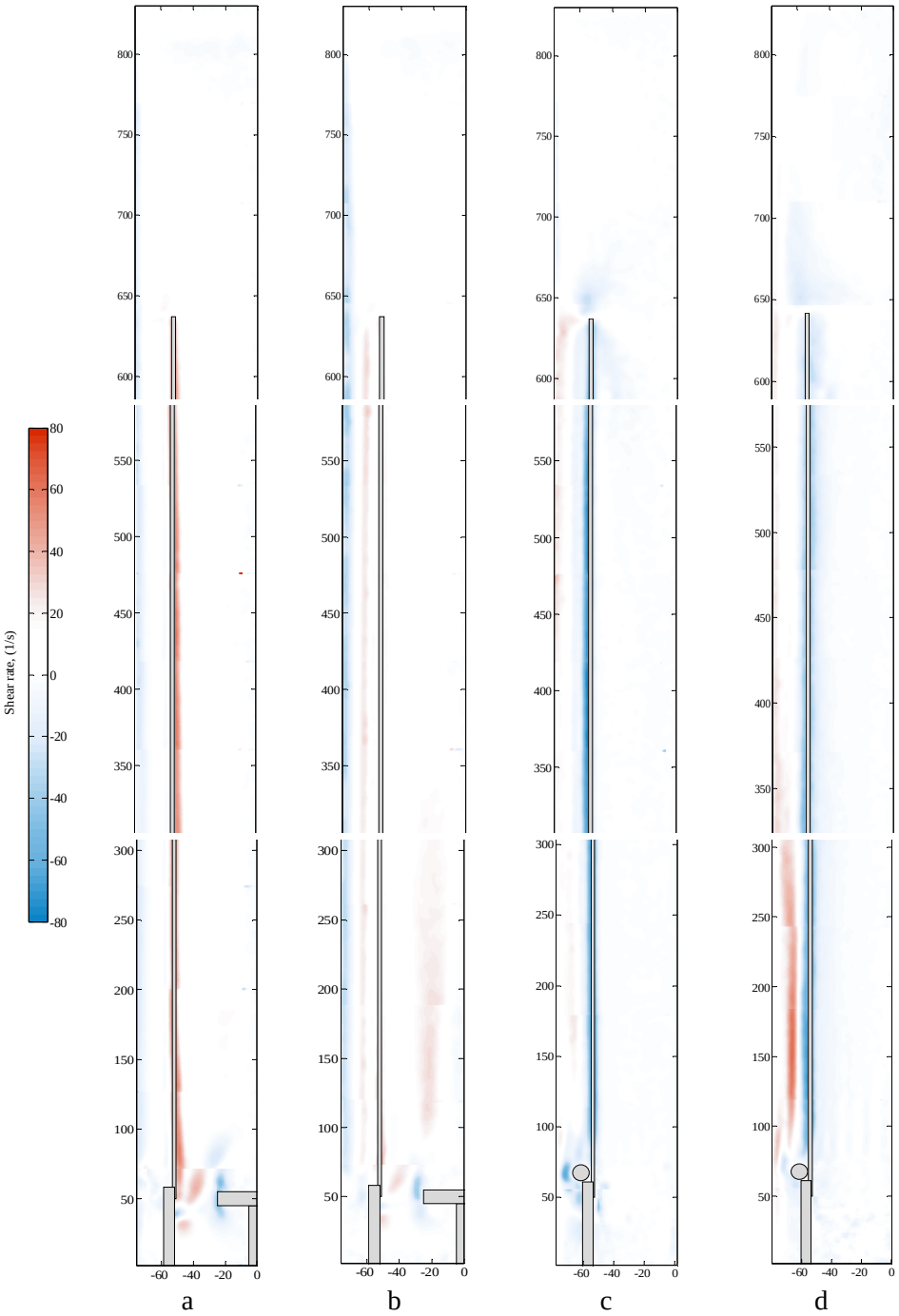


Figure 10. Shear rate fields at $U_g$ 1.18 cm/s: (a) CR-water, (b) CR-model solution, (c) AR-water, (d) AR-model solution.

studies on the gas distribution and mass transfer characteristics, i.e. gas holdup, bubble size, interfacial area, volumetric mass transfer coefficient and liquid-side mass transfer coefficient, were performed in an AR-ALR with non-Newtonian fluids of different apparent viscosities in order to obtain information valuable for the design of suitable reactors and for optimization of aeration conditions (Publication II).

The accuracy of the EIT measurements of the AR-ALR was confirmed by comparing the EIT results to results for the conventional pressure difference method (Publication II, Fig. 3). The EIT results (Publication II, Fig. 4) show that the axial profiles of the local gas holdup in the riser of the AR-ALR become significant at high $U_g$ and liquid apparent viscosity. The gas holdup at the inlet of the downcomer and near the gas distributor is impacted by the draft tube due to the change in liquid flow direction. Cross-sectional gas holdup distributions at a given axial height in the riser were retrieved from experimental data acquired by EIT using an image reconstruction method. Figures 11 and 12 show that gas holdup and gas holdup distribution are promoted by higher superficial gas velocity but the effect is decreased by increasing liquid viscosity. In highly viscous liquid, bubble formation at the gas distributor was even partially prevented, due to viscous drag, and gas holdup and gas holdup distribution in the whole riser clearly declined, as shown in Figures 11 (d) and 12 (d). The reconstructed gas holdup images show the asymmetrical characteristic of the gas distribution in the AR-ALR. This asymmetrical distribution is related to the initial gas distribution, which is determined by the gas distributor and the bubble movement characteristics in the riser of the AR-ALR as well as the influence of liquid viscosity. Thus, one possible solution to promote gas distribution in the AR-ALR could be to improve the initial gas distribution by optimizing the gas distributor structure.

Bubble size distribution (BSD) in water (Publication II, Fig. 8 (b)) is unimodal and becomes broader at high $U_g$. The BSD in non-Newtonian fluids (Publication II, Fig. 8 (b)) with high viscosity (> 0.02 Pa s) become bimodal at high $U_g$. Bubble Sauter mean diameter increases with $U_g$ and liquid apparent viscosity (Publication II, Fig. 9), which is attributed to the number of large bubbles increasing at the expense of small bubbles

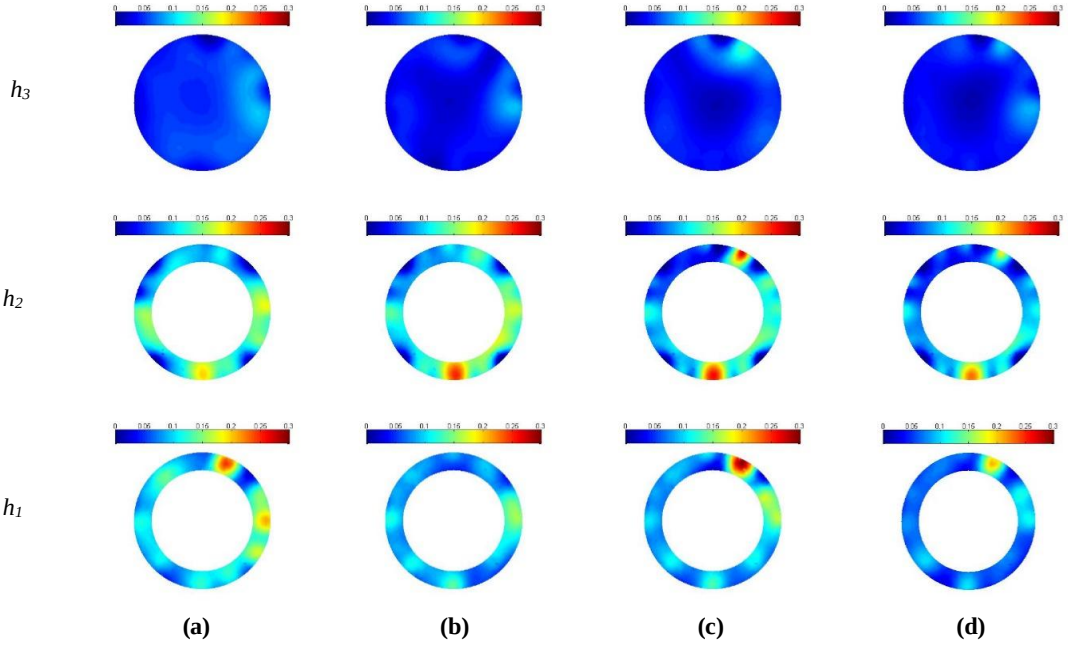


Figure 11. Gas holdup distribution measured by EIT at $U_g$ = 1.18 cm/s in: (a) Water, (b) 0.04 wt.% CMC, (c) 0.07 wt.% CMC, (d) 0.14 wt.% CMC.

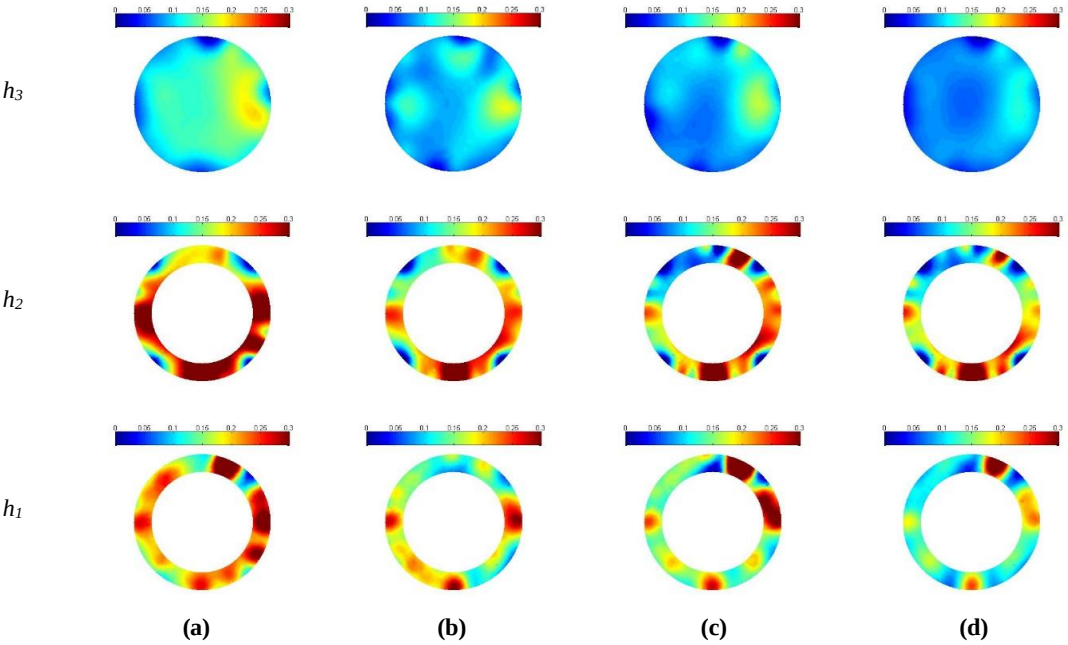


Figure 12. Gas holdup distribution measured by EIT at $U_g$ = 2.55 cm/s in: (a) Water, (b) 0.04 wt.% CMC, (c) 0.07 wt.% CMC, (d) 0.14 wt.% CMC.

along the axial height of the riser. The difference in BSD characteristics in water and CMC solutions implies that bubble coalescence and breakup are much more intensive and complex at high viscosity. The BSD results are also in accordance with the gas holdup distribution characteristics of the different fluids. The interfacial area (Publication II, Fig. 10) between the gas and liquid phases increases linearly with superficial gas velocity and declines with increasing liquid viscosity. Changes in the interfacial area along the axial position become more apparent at high $U_g$ and liquid viscosity (Publication II, Fig. 11). The largest value of the interfacial area is found to appear at the fully developed zone in the riser.

The mass transfer performance is influenced by the hydrodynamics in the AR-ALR. The volumetric mass transfer coefficient is affected positively by increased superficial gas velocity and negatively by increased liquid viscosity, as shown in Figure 13. The influence of the superficial gas velocity on the mass transfer coefficient reduces with increasing liquid viscosity. The results show that $k_La$ increases with superficial gas velocity and the increasing trend declines with increasing CMC concentration. The variation of $k_La$ with $U_g$ is similar to the overall gas holdup in each air-liquid system, although $k_La$ is a little more sensitive to liquid viscosity. This indicates that the gas-liquid

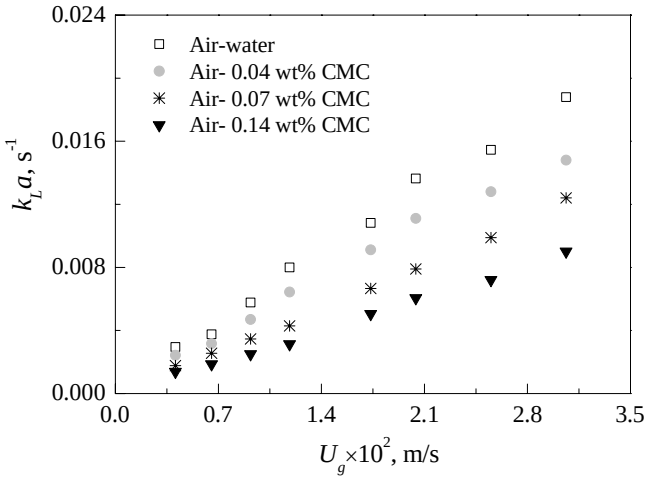


Figure 13. Influence of the superficial gas velocity and solution concentrations on $k_La$.

mass transfer rate is closely related to the overall gas holdup in the AR-ALR and strongly influenced by the liquid viscosity (Publication II, Fig. 2).

Figure 14 gives the liquid-side mass transfer coefficient $k_L$ obtained by dividing the $k_La$ using the average interfacial area. The average interfacial area was evaluated using the overall gas holdup and the average value of the Sauter mean diameter obtained at three axial positions (Eq. 8 in Publication II). Figure 14 shows that first $k_L$ slightly increases with $U_g$ and then becomes insensitive to $U_g$. However, $k_L$ decreases significantly with increasing CMC concentration. The results are in agreement with the study of Yoshimoto *et al.* (2007). It is well known that turbulence intensity increases with $U_g$ and reduces with liquid viscosity. In addition, liquid viscosity also increases mass transfer resistance due to lower diffusivity. Therefore, increasing solution concentration leads to lower $k_L$, while $k_L$ increases with $U_g$ to some extent. The dependence of $k_L$ on $d_{32}$ shows that $k_L$ increases slightly with bubble size in both Newtonian and non-Newtonian fluids. In the studied range, $k_L$ in Newtonian fluids is more sensitive to $d_{32}$ in the homogeneous flow regime, whereas in non-Newtonian fluids it is more sensitive to $d_{32}$ in the heterogeneous flow regime.

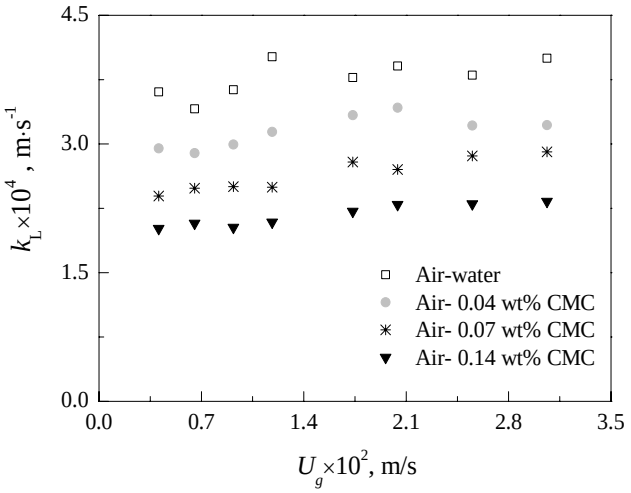


Figure 14. Influence of superficial gas velocity and solution concentrations on $k_L$.

## 4.2 Numerical simulation results

### 4.2.1 Three-phase model of airlift reactors

A three-phase ALR model, that is, an Eulerian model with two bubble phases, was developed to simulate the hydrodynamics and mass transfer of laboratory- and large-scale AR-ALRs operating in the three circulation flow regimes (Publication III). The developed three-phase model was able to capture the three circulation flow regimes of the AR-ALR (Publication III, Fig. 4) in a similar way as observed in experiments. Good agreement for gas holdup (Publication III, Fig. 3) and volumetric mass transfer coefficient (Publication III, Fig. 5) were obtained between the simulations and experiments.

Simulation of a large scale AR-ALR with identical geometrical proportions and 4.5 m height was performed in order to investigate the effect of reactor scale on the hydrodynamics and mass transfer. The simulated overall gas holdup and volumetric mass transfer coefficient agreed well with experimental studies from the literature (Deng *et al.*, 2010). The simulations showed that the average liquid velocities are higher in large-scale AR-ALRs than in laboratory-scale reactors, as shown in Figure 15. A similar result has been reported by van Baten *et al.* (2003), who attributed the difference to reduced frictional losses of the liquid phase in the larger-scale reactor.

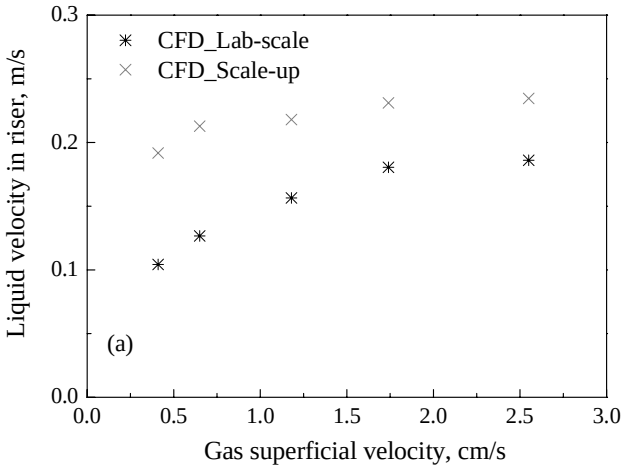

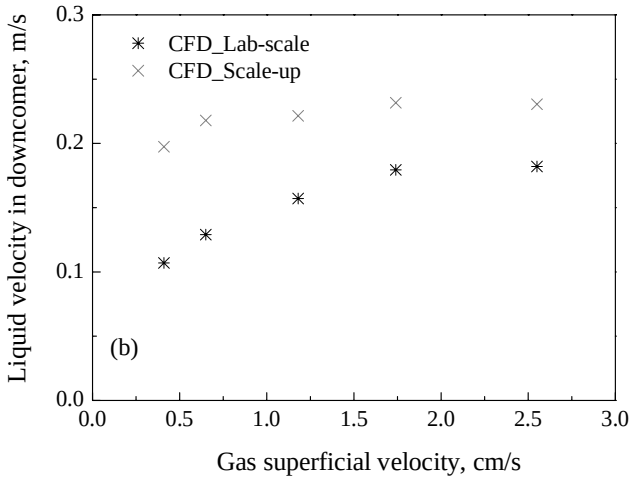


Figure 15. Cross-sectional area averaged liquid velocity at the half of reactor height: (a) in riser, (b) in downcomer.

### 4.2.2 CFD-PBM coupled simulation of an airlift bioreactor

Numerical simulations (Publication IV) were performed with the developed CFD-PBM coupled model of an airlift bioreactor to deepen understanding of the hydrodynamic characteristics of multiphase bioreactors. Local and detailed simulation results can provide valuable information that can contribute to effective design and optimization of ALRs in practical applications. In the numerical simulations, an assumption of two-dimensional axis-symmetry was used based on the geometrical symmetry of the ALR and for reasons of computational costs.

At $U_g$ of 1.18 cm/s, the simulated evolution of bubble size in the ALR is presented in Figure 16 for the air-water and in Figure 17 for the air-CMC system. The bubble size distribution (BSD) at the inlet boundary is given based on experimental measurements for each system, as shown in Figure 16 (a) and 17 (a). It can be seen that the simulated BSD changes only slightly for both the air-water and the air-CMC systems. The BSD characteristics indicate that bubble breakup and coalescence in the ALR is not significant at $U_g$ of 1.18 cm/s due to the low turbulence level. The small increase in the volume fraction of large bubbles results from the contributions of the coalescence kernel models at low $\varepsilon$.

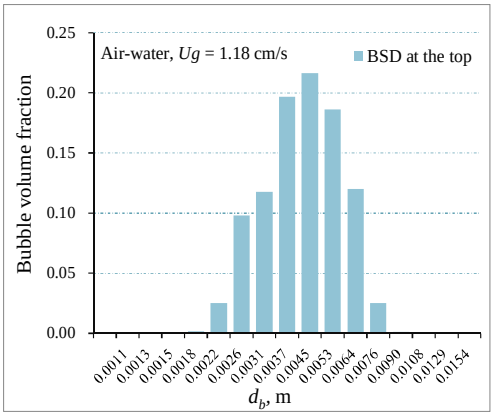


(b)

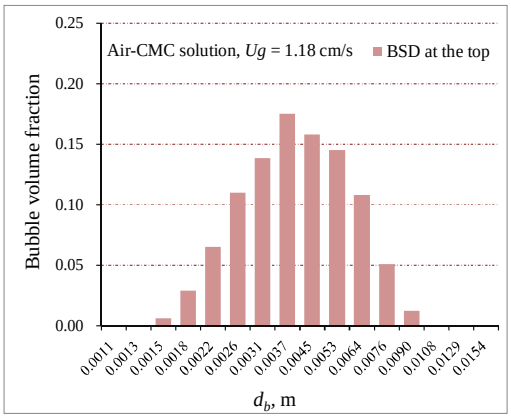


(b)

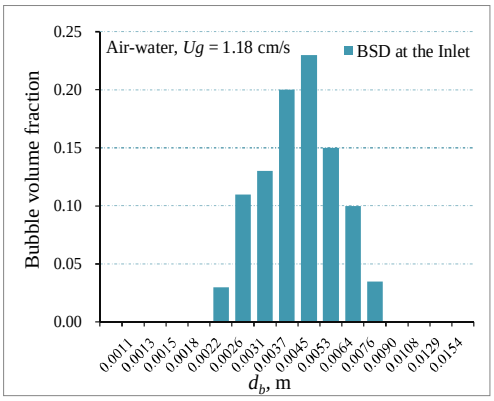


(a)

Figure 16. Evolution of bubble size for air-water in the ALR at $U_g$ of 1.18 cm/s.

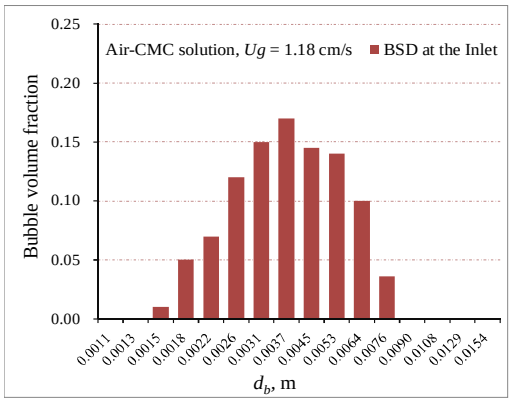


(a)

Figure 17. Evolution of bubble size for air-water in the ALR at $U_g$ of 1.18 cm/s.

With increasing $U_g$, bubble breakup and coalescence rates become considerable for both two-phase systems due to increase in gas holdup and turbulence intensity. Figure 18 shows the evolution of the simulated bubble size in the ALR with air-water at $U_g$ of 2.04 cm/s, where (a) gives the BSD at the inlet boundary evaluated from experiments. The mean bubble size (at which the peak of the volume fraction distribution appears) decreases from 5 to 4 mm and the BSD becomes slightly broader, as shown in Figure 18. This evolution illustrates that bubble breakup due to turbulent collisions is dominating for air-water at $U_g$ of 2.04 cm/s at the top zone of the ALR. Figures 19 (a) and (b) give, respectively, the BSD at the inlet boundary and the simulated BSD at the top zone in the ALR with the air-CMC solution at $U_g$ of 2.04 cm/s. It can be seen that the BSD at the

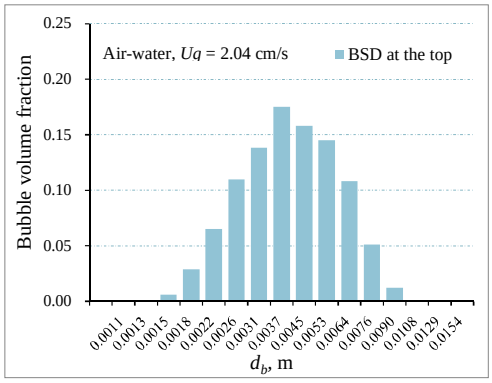


(b)

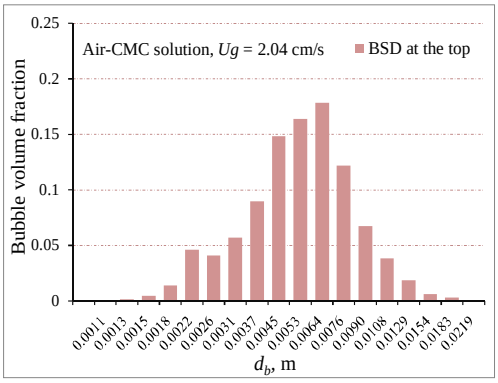


(b)

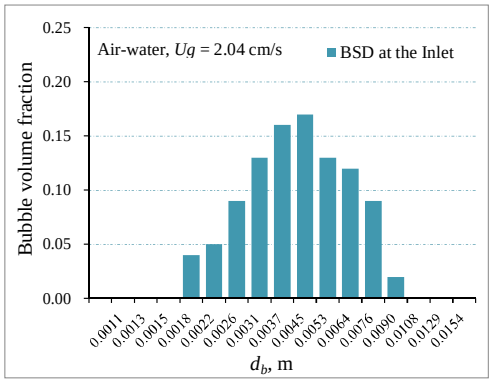


(a)

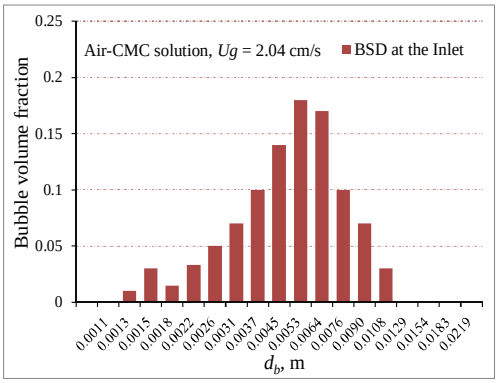


(a)

Figure 18. Evolution of bubble size for air-water in the ALR at $U_g$ of 2.04 cm/s.

Figure 19. Evolution of bubble size for air-water in the ALR at $U_g$ of 2.04 cm/s.

top zone becomes broader and larger bubbles appear at the top zone compared to the inlet. The mean bubble size increases from 5 to 6 mm and the volume fractions of small bubbles (< 2 mm) decrease at the top zone, as shown in Figure 19. The evolution of the bubble size characteristics in the air-CMC solution suggest that bubble coalescence is prevailing for the air-CMC system in the ALR at $U_g$ of 2.04 cm/s. In view of the effect of the different kernel models for the different coalescence mechanisms (see Figure 6), it can be concluded that coalescence due to turbulent collisions probably contributes the greatest part to the simulated bubble sizes. Moreover, coalescence due to wake entrainment and different rise velocities is also considerable, since $c_W$ and $c_U$ is comparable to $c_T$ for those bubbles larger than ~ 6 mm, as shown in Figure 6.

The calculated bubble sizes from the developed CFD-PBM coupled model were compared with experimental measurements at the top zone of the ALR. A fair agreement was obtained for the bubble size distribution (Publication IV, Fig. 5) and for the bubble Sauter mean diameter (Publication IV, Fig. 6). The bubble size is characterized by a narrow distribution in both water and CMC solution at a low superficial gas velocity of 1.18 cm/s (Publication IV, Fig. 5 a) and c)), which is a result of negligible bubble breakup and coalescence due to low gas holdup and turbulent intensity. At higher superficial gas velocity of 2.04 cm/s, however, bubble size distributions became broad in water and even bimodal in the CMC solution (Publication IV, Fig. 5 b) and d)). The bubble Sauter mean diameter is slightly under-predicted in water and over-predicted in CMC solution. These simulated BSD results are most probably obtained because the breakup sub-models in the PBM are much more sensitive to the viscosity (> 0.01 Pa s) compared to the coalescence models (Xing *et al.*, 2013). The simulated overall gas holdup (Publication IV, Fig. 4) increases with superficial gas velocity and is higher in air-water than in air-CMC solution at identical $U_g$, which matches well with the experiments. The radial profiles of the axial liquid velocity are more uniform for air-water than for the air-CMC solution, particularly in the downcomer, which is predicted well with the developed model. The liquid velocity profile at the top of the ALR (Publication IV, Fig. 9 - 10) is notably different in the air-water system than in the air-CMC solution at high $U_g$, which might be attributable to the effects of movement of large bubbles and bubble wakes.

The velocity fields for the simulations and experiments are compared for the air-water system at $U_g$ of 2.04 cm/s in Figure 19 and for the air-CMC solution in Figure 20. When compared with PIV measurements, the velocity fields of the gas and liquid phases are generally well predicted with the developed CFD-PBM coupled model. The liquid flow structure at the top of the ALR in the air-water system (Figure 19 (a) and (c)) is clearly different from that in the air-CMC solution (Figure 20 (a) and (c)), as seen in both the PIV measurements and numerical simulations. The well-matched results between the simulations and experiments indicate that for the investigated conditions, the developed CFD-PBM model is able to describe the hydrodynamics in the ALR with reasonable accuracy.

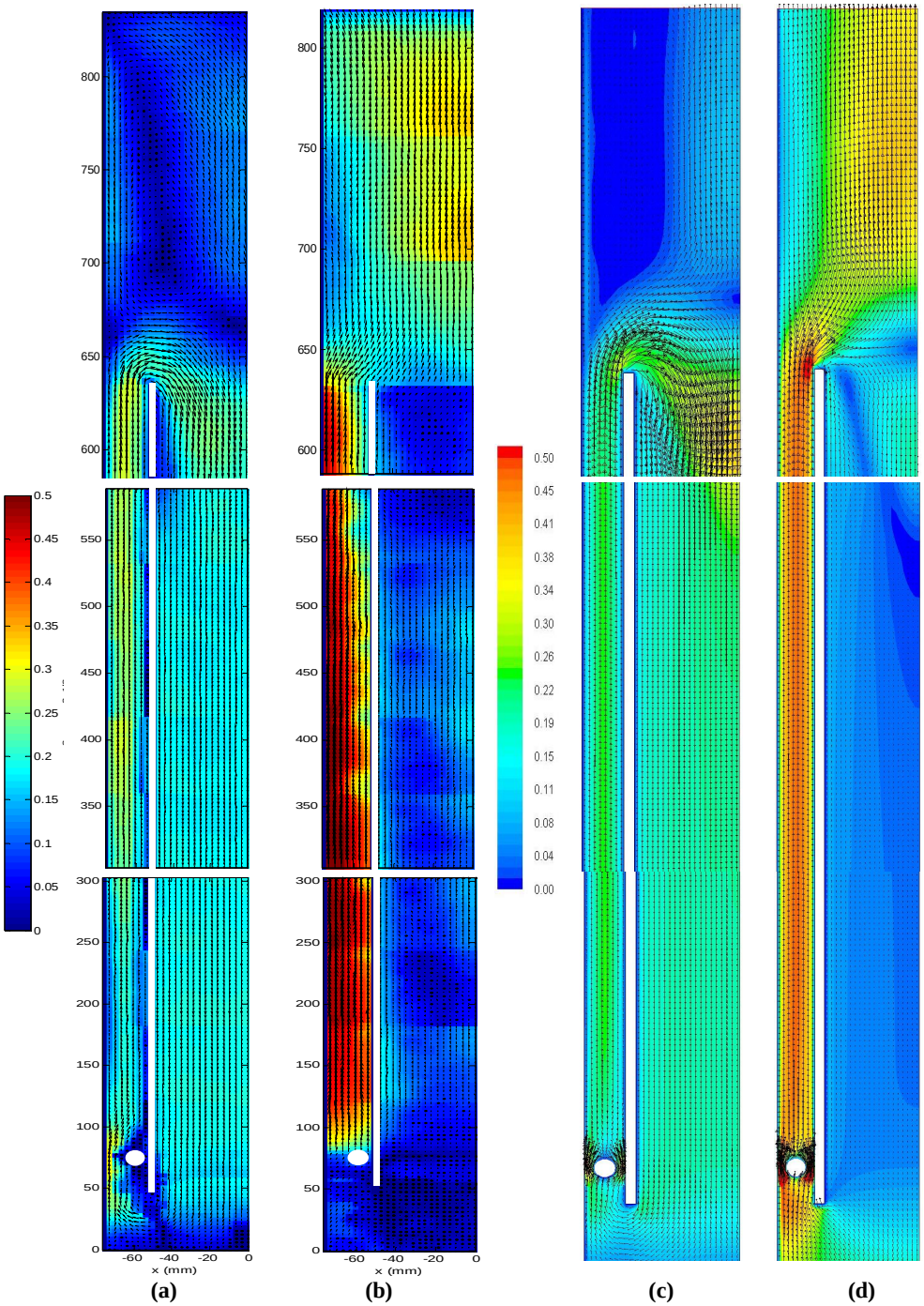


Figure 19. Velocity fields of AR-ALR with water at $U_g$=2.04 cm/s:
(a) liquid velocity - PIV, (b) gas velocity - PIV, (c) liquid velocity - simulation,
(d) gas velocity - simulation.

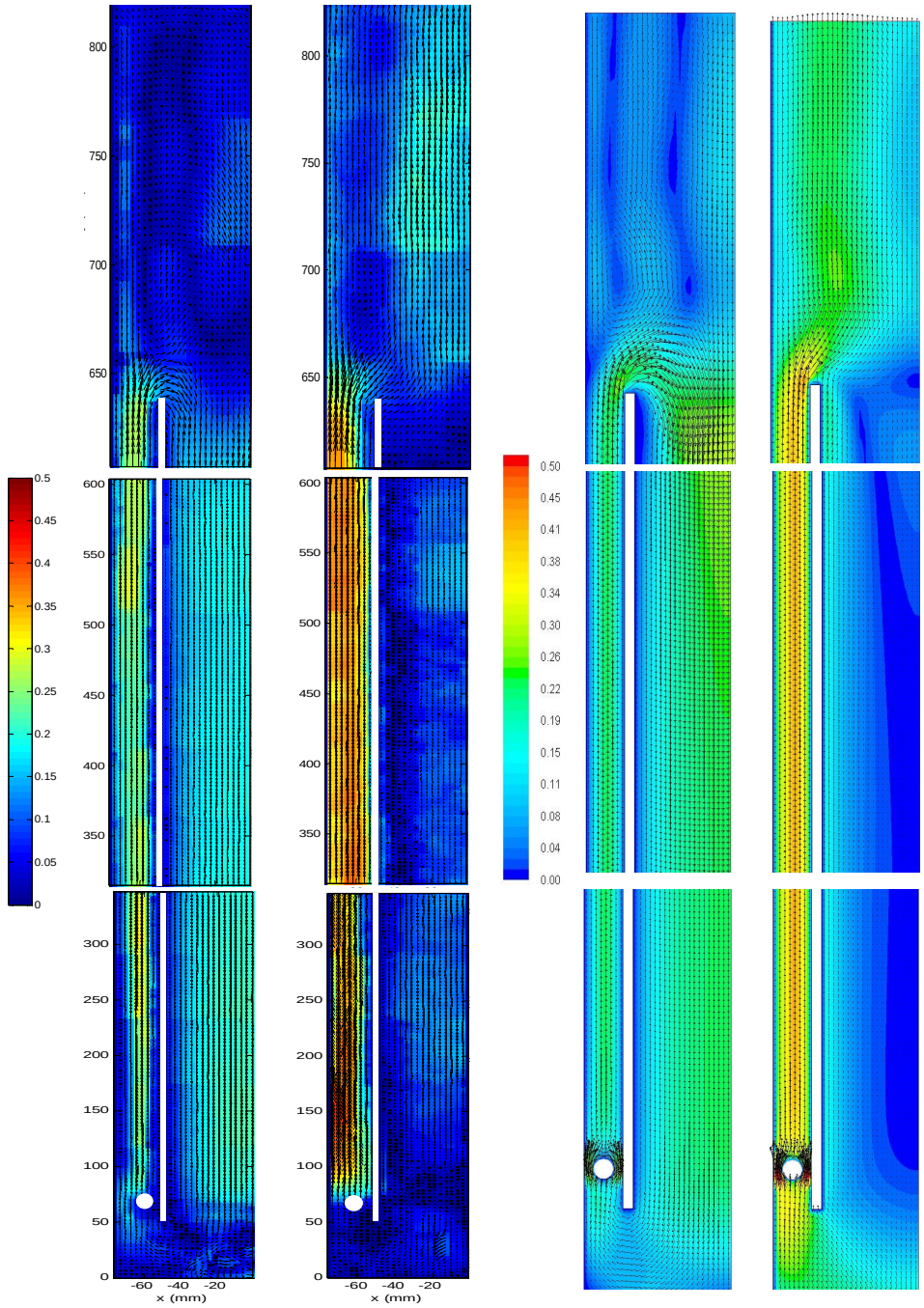


Figure 20. Velocity fields of AR-ALR with CMC solution at $U_g$ 2.04 cm/s: (a) liquid velocity - PIV, (b) gas velocity - PIV, (c) liquid velocity - simulation, (d) gas velocity - simulation.

## 5. Conclusions

In this thesis, hydrodynamics and mass transfer in the airlift bioreactor were studied experimentally and with numerical simulation. Hydrodynamics and mass transfer are important factors that directly determine reactor performance. Experimental results from novel and advanced measurement techniques provided valuable hydrodynamic data for airlift bioreactors and brought new insights into potential approaches for improvement of mass transfer. Numerical models were developed for airlift bioreactors for low viscous Newtonian fluids and viscous non-Newtonian fluids respectively. In the models developed, bubble size characteristics are taken into account using the simplified two-class model and PBM, respectively. The simulation results are well matched with experimental values and give improved understanding of the flow mechanisms behind multiphase flow in airlift bioreactors. The findings provide valuable information enabling improved reactor design, scale-up and optimization.

Detailed experimental investigations and comparisons of center-rising and annulus-rising airlift bioreactors are presented in the thesis. This work improves understanding of the pros and cons of the two aeration modes, thus enabling appropriate selection of airlift reactor type and facilitating effective utilization of airlift bioreactors. The results show that the annulus-rising airlift bioreactor performs better than the center-rising airlift bioreactor in terms of overall gas holdup, mass transfer and foam layer thickness (Publication I, Figure 2.). As a trade-off between high gas holdup and fast mixing, the liquid circulation time in the annulus-rising airlift bioreactor is longer than in the center-rising reactor. Novel and interesting results concerning different liquid circulation structures and shear rate fields were found for the center-rising and annulus-rising airlift bioreactors. Greater knowledge of local hydrodynamics will aid researchers and engineers in further research and development of airlift bioreactors.

Mass transfer characteristics and local gas holdup distributions were experimentally studied in an annulus-rising airlift bioreactor for non-Newtonian fluids, which are commonly encountered in industry. Novel visualized results of gas distribution and local

gas holdup were obtained by introducing and applying a three-dimensional electrical impedance tomography method, thus bringing new insights into potential approaches for improving aeration and enhancing gas-liquid contact. The local measurement results showed that the changes in gas hydrodynamics in the axial direction become significant at high superficial gas velocity and apparent viscosity. The maximum value for the local gas holdup and the interfacial area was found at the fully developed flow zone in the middle of the riser. The uniformity of the gas distribution was reduced significantly by increased liquid viscosity. This non-uniformity could be slightly improved by increasing the superficial gas velocity. A possible effective solution to promote greater uniformity of the gas distribution could be to improve the initial gas distribution by optimizing the gas distributor structure.

The liquid-side mass transfer coefficient and the gas-liquid interfacial area were investigated separately, which gives better understanding of mass transfer and hydrodynamics in airlift bioreactors. It was found that the liquid-side mass transfer coefficient in an airlift reactor is mostly dependent on the liquid viscosity and bubble size rather than the superficial gas velocity.

Computational fluid dynamics simulation can predict airlift bioreactors accurately provided that the numerical model used describes the physical phenomena of the multiphase flow well. In the current research, a three-phase model for airlift bioreactors was developed for low viscous Newtonian fluids that was able to predict the hydrodynamics and mass transfer well over three circulation flow regimes. The developed three-phase model was capable of giving reasonable predictions for the effect of reactor scale, which were verified by comparison to experiments in published literature. Additionally, a computational fluid dynamics model for airlift bioreactors in which wide bubble size distribution, attributed to bubble coalescence and breakup, is taken into account was developed for non-Newtonian fluids in order to improve the confidence of the model predictions. Simulations showed that the liquid flow structure at the top of the reactor differs for the air-non-Newtonian fluid system and the air-Newtonian fluid system, which matches well with experimental data. Good agreement on bubble size, overall gas

holdup and velocity fields between the experimental and simulated results was found. This good agreement suggests that the developed computational fluid dynamics model is able to describe and predict the hydrodynamics in an airlift bioreactor with non-Newtonian fluids with reasonable accuracy.

## 6. Suggestions for future work

Inadequate gas-liquid mass transfer is considered as one of the main factors preventing commercialization of many green technologies. Effective and economic solutions for improved mass transfer of sparingly soluble gases in industrial airlift bioreactor applications are sorely needed. The aim of improving mass transfer in bioreactors forms the background to the current research, and it will most likely be the main driver of future research work in airlift bioreactor applications. This objective can probably be best achieved by improving the hydrodynamics in airlift bioreactors.

Experimental results show that the mass transfer rate in annulus-rising airlift reactors is higher than in center-rising airlift bioreactors, which is attributed mainly to the amount of bubbles dragged into the downcomer and the higher gas holdup in annulus-rising airlift bioreactors. Therefore, alteration of the flow regime in which the reactor operates, e.g. promotion of circulation flow regime III, may enhance mass transfer, since it enables an increase in the gas residence time and the specific interfacial area in the reactor. Additionally, investigation of mass transfer and hydrodynamics of gas-liquid-solid systems operated in airlift bioreactors is required. Comprehensive understanding of such systems is needed by both industry and academia.

The computational fluid dynamics model developed in this thesis considers the multiple breakup and coalescence mechanisms and several bubble size groups in order to better describe the bubble characteristics in airlift bioreactors. Thus, relatively large computing resources are needed for the developed model with discretized PBM to calculate the BSD and hydrodynamics, especially for large scale ALRs. To achieve better prediction of airlift bioreactors with more economical use of computational resources, further studies on bubble breakup and coalescence behavior in non-Newtonian fluids are essential, including sub-models for bubble breakup and coalescence and comprehensive bubble size data. More efficient numerical methods are required to calculate the PBM and to couple the PBM with computational fluid dynamics models.

## References

Alopaeus, V., Keskinen I.K., Koskinen J., Majander J., Pitkänen H., Holma H., Gas-liquid stirred tank reactor modelling with CFD and user subroutines, AIChE Annual Meeting, October 3-8, 2002, Indianapolis, the United State of America.

Abdullah B., Dave C., Nguyen T.H., Cooper C.G., Adesina A.A., Electrical resistance tomography-assisted analysis of dispersed phase hold-up in a gas-inducing mechanically stirred vessel, Chem. Eng. Sci., 2011, 66, 5648-5662.

Acrivos A., The breakup of small drops and bubbles in shear flows, Annals New York Academy of Science, 1983, 404, 1-11.

Ahamed A., Vermette P., Culture-based strategies to enhance cellulase enzyme production from *Trichoderma Reesei* RUT-C30 in bioreactor culture conditions, Biochem. Eng. Journal, 2008, 40, 399- 407.

Ali R.M., Jamel C., Ghazi B., Line A., Gas dispersion in air-lift reactors: contribution of the turbulent part of the added mass force, AIChE J., 2011, 57, 3315-3330.

Amooghin A.E., Jafari S., Sanaeepur H., Kargari A., Computatinal fluid dynamics simulation of bubble coalescence and breakup in an internal airlift reactor: Analysis of effects of a draft tube on hydrodynamics and mass transfer, Appl. Math. Mod. 2015, 39, 1616-1642.

Bergault I., Joly-Vuillemin C., Fouilloux P., Delmas H., Modeling of acetophenone hydrogenation over a Rh/C catalyst in a slurry airlift reactor, Catalysis Today, 1999, 48, 161-174.

Berovic M., Bioreactors in Biotechnology, Doelle H.W., Rokem J.S., Berovic M., Eds., 2009, Oxford: Eolss.

Blažej M., Kiša M., Markoš J., Scale influence on the hydrodynamics of an internal loop airlift reactor, Chem. Eng. Proc., 2004, 43, 1519-1527.

Bhole M.R., Joshi J.B., Ramkrishna D., CFD simulation of bubble columns incorporating population balance modeling, Chem. Eng. Sci., 2008, 63, 2267-2282.

Cockx. A., Quang Z. D., Audic J. M., Liné A., Roustan M., Global and local mass transfer coefficients in the waste water treatment process by computational fluid dynamics, Chem. Eng. Process., 2001, 40, 187-194.

Chatzi, G.E., Gavrielides D.A., Kiparissides C., Generalized model for prediction of the steady-state drop size distributions in batch stirred vessels, Ind. Eng. Chem. Res., 1989, 28, 1704–1711.

Chavez-Parga M. C., Gonzalez-Ortega O., Negrete-Rodriguez M. L. X., Medina-Torres L., Escamilla-Silva E. M., Hydrodynamics, mass transfer and rheological studies of gibberellic acid production in an airlift bioreactor, World J. Microb. Biot., 2007, 23, 615-623.

Chavez-Parga M. C., Gonzalez-Ortega O., Negrete-Rodriguez M. L. X., Vallarino I. G., Alatorre G. G., Escamilla-Silva E. M., Kinetic of the gibberellic acid and bikaverin production in an airlift bioreactor, Process Bio-chem., 2008, 43, 855-860.

Chen P., Sanyal J., Duduković, Numerical simulation of bubble column flows: effect of different breakup and coalescence closures, Chem. Eng. Sci., 2005, 60, 1085- 1101.

Chisti M.Y., Airlift Bioreactors, 1989, London: Elsevier.

Deen, N.G., Hjertager, B.H. & Solberg, T., Comparison of PIV and LDA Measurement Methods Applied to the Gas-Liquid Flow in a Bubble Column, 10th International Symposium on Applications of Laser Techniques to Fluid Mechanics, July 10-13, 2000, Lisbon, Portugal.

Deen N.G., Westerweel J., Hjertager B.H., Upper limit of the gas fraction in PIV measurements in dispersed gas-liquid flows, 5th International Conference on Gas-Liquid and Gas-Liquid-Solid Reactor Engineering, September 23-27, 2001, Melbourne, Australia.

Deng Z.H., Wang T.F., Zhang N., Wang Z.W., Gas holdup, bubble behavior and mass transfer in a 5 m high internal-loop airlift reactor with non-Newtonian fluid, Chem. Eng. J., 2010, 160, 729-737.

Dhanasekharan K.M., Sanyal J., Jain A., Haidari A., A generalized approach to model oxygen transfer in bioreactors using population balances and computational fluid dynamics, Chem. Eng. Sci., 2005, 60, 213-218.

Elemans, P.H.M., Bos H.L., Janssen J.M.H., Meijer H.E.H., Transient phenomena in dispersive mixing, Chem. Eng. Sci., 1993, 48, 267-276.

Eloranta H., Honkanen M., Marjanen K., PORA-Object Recognition and Analysis Software 1.0 Users Manual, Version 1.0/9.9.2008, © Pixact Ltd., www.pixact.fi.

Fu X.Y., Ishii M., Two-group interfacial area transport in vertical air-water flow I. Mechanistic model, Nucl. Eng. Des., 2002, 219, 143-168.

Fujiwara A., Minato D., Hishida K., Effect of bubble diameter on modification of turbulence in an upward pipe flow, Inter. J. Heat Fluid Flow, 2004, 25, 481-488.

Ge C.Y., Wang J.J., Gu X.P., Feng L.F., CFD simulation and PIV measurement of the flow field generated by modified pitched blade turbine impellers, Chem. Eng. Res. Des., 2014, 92, 1027-1036.

González G., Huttunen J.M.J., Kolehmainen V., Seppänen A., Vauhkonen M., Experimental evaluation of 3D electrical impedance tomography with total variation prior, Inverse Probl. Sci. Eng., 2015, 24, 1411-1431.

Grace H.P., Dispersion phenomena in high viscosity immiscible fluid systems and application of static mixers as dispersion devices in such systems, Chem. Eng. Commun., 1982, 14, 225-277.

Gumery F., Ein-Mozaffari F., Dahman Y., Macromixing hydrodynamic study in draft-tube airlift reactors using electrical resistance tomography, Bioprocess Biosyst. Eng., 2011, 34, 135-144.

Hamood-ur-Rehman M., Ein-Mozaffari F., Dahman Y., Dynamic and local gas holdup studies in external loop recirculating airlift reactor with two rolls of fiberglass packing using electrical resistance tomography, J. Chem. Technol. Biotechnol., 2013, 88, 887-896.

Heijnen J.J., Hols J., van der Lans R.G.J.M., van Leeuwen H.L.J.M., Mulder A., Weltevrede R., A simple hydrodynamic model for the liquid circulation velocity in a full-scale two- and three-phase internal airlift reactor operating in the gas recirculation regime, Chem. Eng. Sci., 1997, 52, 2527- 2540.

Hekmat A., Amooghin A.E., Moraveji M.K., CFD simulation of gas-liquid flow behaviour in an air-lift reactor: determination of the optimum distance of the draft tube, Simulation Modelling Practice and Theory, 2010, 18, 927-945.

Hinze J.O., Fundamentals of the hydrodynamic mechanism of splitting in dispersion process, AIChE J. 1955, 1, 289-295.

Hosokawa S., Tomiyama A., Bubble-induced pseudo turbulence in laminar pipe flows, Int. J. of Heat Fluid Fl., 2013, 40, 97-105.

Huang Q.S., Yang C., Yu G.Z., Mao Z.S., 3-D simulation of an internal airlift loop reactor using a steady two-fluid model, Chem. Eng. Technol., 2007, 30, 870-879.

Huang Q.S., Yang C., Yu G.Z., Mao Z.S., CFD simulation of hydrodynamics and mass transfer in an internal airlift loop reactor using a steady two-fluid model, Chem. Eng. Sci., 2010, 65, 5527-5536.

Huang Q.S., Zhang W.P., Yang C., Modeling transport phenomena and reactions in a pilot slurry airlift loop reactor for direct coal liquefaction, Chem. Eng. Sci., 2015, 135, 441-451.

Howarth W.J., Coalescence of drops in a turbulent flow field, Chem. Eng. Sci., 1964, 33-38.

Jacobsen H.A., Sannaes B.H., Grevskott S., Svendsen H.F., Modeling of vertical bubble-driven flows, In. Eng. Chem. Res., 1997, 36, 4052-4074.

Jafari Nasr M.R., Bakhtiary H.R., Karimi A., Tavassoli A., Single step H2S removal using chelated iron solution investigation of hydrodynamic parameters in an internal loop airlift reactor, Iranian J. Sci. Technol. 2004, 28, 643-651.

Jakobsen H., On the modeling and simulation of bubble column reactors using a two-fluid model, PhD thesis, Norweigian Institute of Technology, Norway, 1993, 110p.

Klein J., Vicente A.A., Teixeira J., Hydrodynamics of a three-phase airlift reactor with an enlarged separator-application to high cell density systems., Can. J. Chem. Eng., 2003, 81, 433-443.

Koide K., Kurematsu K., Iwamoto S., Iwata Y., Horibe K., Gas holdup and volumetric liquid-phase mass transfer coefficient in bubble column with draught tube and with gas dispersion into annulus, J. Chem. Eng. Jap., 1983, 16, 407-413.

Kourunen J., Savolainen T., Lehikoinen A., Vauhkonen M., Suitability of a PXI platform for an electrical impedance tomography system, Measurement Sci. Tech., 2009, 20, 1-11.

Lahey R.T., Lopez de Bertodano M., Jones O.C., Phase distribution in complex geometry conduits, Nuclear Eng. Des., 1993, 141,177-201.

Lehr F., Mewes D., A transport equation for the interfacial area density applied to bubble columns, Chem. Eng. Sci., 2001, 56, 1159-1166.

Lehr F., Millies M., Mewes D., Bubble-size distributions and flow fields in bubble columns, AIChE J., 2002, 48, 2426-2443.

Lennartsson P. R., Niklasson C., Taherzadeh M. J., A pilot study on lignocellulose to ethanol and fish feed using NMMO pretreatment and cultivation with zygomycetes in an air-lift reactor, Bioresour. Tech., 2011, 102, 4425-4432.

Lestinsky P., Vecer M., Vayrynen P., Wichterle K., The effect of the draft tube geometry on mixing in a reactor with an internal circulation loop – A CFD simulation, Chem. Eng. Proc., 2015, 94, 29-34.

Liao Y.X., Lucas D., A literature review of theoretical models for drop and bubble breakup in turbulent dispersions, Chem. Eng. Sci., 2009, 64, 3389-3406.

Liao Y.X., Lucas D., A literature review on mechanisms and models for the coalescence process of fluid particles, Chem. Eng. Sci., 2010, 65, 2851-2864.

Lin T.J., Chen P.C., Studies on hydrodynamics of an internal-loop airlift reactor in gas entrainment regime by particle image analyzer, Chem. Eng. J., 2005, 108, 69-79.

Liu R., Sun W., Liu C.Z., Computational fluid dynamics modelling of mass transfer behaviour in a bioreactor for hair root culture. I. Model development and experimental validation, AIChE J., 2011a, 1661-1671.

Liu R., Sun W., Liu C.Z., Computational fluid dynamics modelling of mass transfer behaviour in a bioreactor for hair root culture. II. Analysis of Ultrasound-Intensified process, AIChE J., 2011b, 1672-1679.

Liu R., Liu Y.., Liu C.Z., Development of an efficient CFD-simulation method to optimize the structure parameters of an airlift sonobioreactor, Chem. Eng. Res. Des., 2013, 91, 211-220.

Lo C.S., Hwang S.J., Local hydrodynamic properties of gas phase in an internal-loop airlift reactor, Chem. Eng. J., 2003, 91, 3-32.

Lopez de Bertodano M., Lahey R.T., Jones O.C., Development of a k-epsilon model for bubbly two-phase flow, J. Fluid Eng., 1994, 116, 128-134.

Luo H.P., Al-Dahhan M., Local characteristics of hydrodynamics in draft tube airlift bioreactor, Chem. Eng. Sci., 2008, 63, 3057-3068.

Luo H.P., Al-Dahhan M.H., Local gas holdup in a draft tube airlift bioreactor, Chem. Eng. Sci., 2010, 65, 4503-4510.

Luo H.P., Al-Dahhan M.H., Verification and validation of CFD simulations for local flow dynamics in a draft tube airlift bioreactor, Chem. Eng. Sci., 2011, 66, 907-923.

Luo H., Svendsen H.F., Theoretical model for drop and bubble breakup in turbulent dispersions, AIChE J., 1996, 42, 1225-1233.

Moravji M.K., Sajjadi B., Jafarkhani M., Davarnejad R., Experimental investigation and CFD simulation of turbulence effect on hydrodynamic and mass transfer in a packed bed airlift internal loop reactor, Inter. Comm. Heat Mass Tran., 2011, 38, 518-524.

Mudde R.F., van den Akker H.E.A., 2D and 3D simulation of an internal airlift loop reactor on the basis of a two-fluid model, Chem. Eng. Sci., 2001, 56, 6351-6358.

Munasinghe P.C., Khanal S.K., Syngas fermentation to biofuel: evaluation of carbon monoxide mass transfer coefficient ($k_L$a) in different reactor configurations, AIChE J., 2015, 26, 1616-1621.

Politano M., Carrica P., Vonverti J., A model for turbulent polydisperse two=phase flow in vertical channels, Int. J. Multiph. Flow 2003, 29, 1153-1182.

Prince M.J., Blanch H.W., Bubble coalescence and break-up in air-sparged bubble columns, AIChE J., 1990, 36, 1485-1499.

Rzehak R., Krepper E., CFD modelling of bubble-induced turbulence, Inter. J. Multiphase Flow, 2013 a, 55, 138-155.

Rzehak R., Krepper E., Bubble-induced turbulence: Comparison of CFD models, Nucl. Eng. Des., 2013 b, 258, 57-65.

Sato Y., Sadatomi M., Sekoguchi K., Momentum and heat transfer in two-phase bubble flow-I. Int. J. Multiph. Flow, 1981, 7, 167-177.

Šimčík M., Mota A., Ruzicka M.C., Vicente A., Teixeira J., CFD simulation and experimental measurement of gas holdup and liquid interstitial velocity in internal loop airlift reactors, Chem. Eng. Sci., 2011, 66, 3268-3279.

Shinnar R., Church J.M., Predicting particle size in agitated dispersions, Indus. Eng. Chemistry, 1960, 52, 253-256.

Tabib M.V., Roy S.A., Joshi J.B., CFD simulation of bubble column – An analysis of interphase forces and turbulence models, Chem. Eng. J., 2008, 139, 589-614.

van Baten J.M., Ellenberger J., Krishna R., Using CFD to describe the hydrodynamics of internal air-lift reactors, Can. J. Chem. Eng., 2003, 81, 660-668.

Versteeg H.K., Malalasekera W., An introduction to Computational fluid dynamics: The finite volume method, 1995, London: Longman.

Vial C., Poncin S., Wild G., Midoux M., Experimental and theoretical analysis of the hydrodynamics in the riser of an external loop airlift reactor, Chem. Eng. Sci., 2002, 57, 4745-4762.

Wang M., Ma Y.X., Holliday N., Dai Y.F., Williams R.A., Lucas G., A high-performance EIT system, IEEE SENSORS J., 2005, 5, 289-299.

Wang T.F., Wang J.F., Jin Y., A novel theoretical breakup kernel function for bubbles/droplets in a turbulent flow. Chem. Eng. Sci., 2003, 58, 4629-4637.

Wang T.F., Wang J.F., Jin Y., Population balance model for gas-liquid flows: influence of bubble coalescence and breakup models, In. Eng. Chem. Res., 2005a, 44, 7540-7549.

Wang T.F., Wang J.F., Jin Y., Theoretical prediction of flow regime transition in bubble columns by the population balance model, Chem. Eng. Sci., 2005b, 60, 6199-6209.

Wilkinson P.M., Vanschayk A., Spronken J.P.M., Vandierendonck L.L., The influence of gas-density and liquid properties on bubble breakup, Chem. Eng. Sci., 1993, 48, 1213-1226.

Wu Q., Wang X.K., Han M., Wang T.F., Sha Z.L., Wang J.F., Axial and radial profiles of hydrodynamic parameters of external-loop airlift reactor, Chinese J. Chem. Eng., 2009, 60, 1427-1434.

Wu X., Merchuk J.C., Measurement of fluid flow in the downcomer of an internal loop airlift reactor using an optical trajectory-tracking system, Chem. Eng. Sci., 2003, 58, 1599-1614.

Xing C.T., Wang T.F., Wang J.F., Experimental study and numerical simulation with a coupled CFD-PBM model of the effect of liquid viscosity in a bubble column, Chem. Eng. Sci., 2013, 95, 313-322.

Yoshimoto M., Suenaga S., Furumoto K., Fukunaga K., Nakao K., Gas-liquid interfacial area, bubble size and liquid-phase mass transfer coefficient in a three-phase external loop airlift bubble column, Chem. Biochem. Q., 2007, 21, 365-372.

Zhang X., Zhou B., Zhang Y., Cai Z., Cong W., Ou-Yang F., A simple and low-cost airlift photobioreactor for microalgal mass culture, Biotech. Letters, 2002, 24, 1767-1771.

Zhao H., Ge W., A theoretical bubble breakup model for slurry beds or three-phase fluidized beds under high pressure, Chem. Eng. Sci., 2007, 62, 109-115.

# Publication I

Han, M., Laari, A., and Koiranen, T.
**Effect of aeration mode on the performance of centre- and annulus-rising internal-loop airlift bioreactors**

Reprinted with permission from
*The Canadian Journal of Chemical Engineering*
In Press (DOI: 10.1002/cjce.22943)

# Publication II

Han M., González G., Vauhkonen M., Laari A., and Koiranen T.
**Local gas distribution and mass transfer characteristics in an annulus-rising airlift reactor with non-Newtonian fluid**

Reprinted with permission from
*Chemical Engineering Journal*
Vol. 308, pp. 929-939, 2017

# Publication III

Han, M., Laari, A., and Koiranen, T.
**Hydrodynamics and mass transfer performance of annulus-rising airlift reactor – the effect of reactor scale**

Reprinted with permission from
*International Journal of Chemical Engineering and Applications*
Vol. 8, pp. 47-52, 2017

# Publication IV

Han, M., Sha, Z.L., Laari, A., and Koiranen, T.
**CFD-PBM coupled simulation of an airlift reactor with non-Newtonian fluid**

Reprinted with permission from
*Oil & Gas Science and Technology – Revue d'IFP Energies nouvelles*
Vol. 72, pp. 1-12, 2017

**ACTA UNIVERSITATIS LAPPEENRANTAENSIS**

**744.** BIBOV, ALEKSANDER. Low-memory filtering for large-scale data assimilation. 2017. Diss.

**745.** ROTICH, NICOLUS KIBET. Development and application of coupled discrete and continuum models in solid particles classification. 2017. Diss.

**746.** GAST, JOHANNA. The coopetition-innovation nexus: Investigating the role of coopetition for innovation in SMEs. 2017. Diss.

**747.** KAPOOR, RAHUL. Competition and disputes in the patent life cycle. 2017. Diss.

**748.** ALI-MARTTILA, MAAREN. Towards successful maintenance service networks – capturing different value creation strategies. 2017. Diss.

**749.** KASHANI, HAMED TASALLOTI. On dissimilar welding: a new approach for enhanced decision-making. 2017. Diss.

**750.** MVOLA BELINGA, ERIC MARTIAL. Effects of adaptive GMAW processes: performance and dissimilar weld quality. 2017. Diss.

**751.** KARTTUNEN, JUSSI. Current harmonic compensation in dual three-phase permanent magnet synchronous machines. 2017. Diss.

**752.** SHI, SHANSHUANG. Development of the EAST articulated maintenance arm and an algorithm study of deflection prediction and error compensation. 2017. Diss.

**753.** CHEN, JIE. Institutions, social entrepreneurship, and internationalization. 2017. Diss.

**754.** HUOTARI, PONTUS. Strategic interaction in platform-based markets: An agent-based simulation approach. 2017. Diss.

**755.** QU, BIN. Water chemistry and greenhouse gases emissions in the rivers of the "Third Pole" / Water Tower of Asia". 2017. Diss.

**756.** KARHU, PÄIVI. Cognitive ambidexterity: Examination of the cognitive dimension in decision-making dualities. 2017. Diss.

**757.** AGAFONOVA, OXANA. A numerical study of forest influences on the atmospheric boundary layer and wind turbines. 2017. Diss.

**758.** AZAM, RAHAMATHUNNISA MUHAMMAD. The study of chromium nitride coating by asymmetric bipolar pulsed DC reactive magnetron sputtering. 2017. Diss.

**759.** AHI, MOHAMADALI. Foreign market entry mode decision-making: Insights from real options reasoning. 2017. Diss.

**760.** AL HAMDI, ABDULLAH. Synthesis and comparison of the photocatalytic activities of antimony, iodide and rare earth metals on SnO2 for the photodegradation of phenol and its intermediates under UV, solar and visible light irradiations. 2017. Diss.

**761.** KAUTTO, JESSE. Evaluation of two pulping-based biorefinery concepts. 2017. Diss.

**762.** AFZALIFAR, ALI. Modelling nucleating flows of steam. 2017. Diss.

**763.** VANNINEN, HEINI. Micromultinationals - antecedents, processes and outcomes of the multinationalization of small- and medium-sized firms. 2017. Diss.

**764.** DEVIATKIN, IVAN. The role of waste pretreatment on the environmental sustainability of waste management. 2017. Diss.

**765.** TOGHYANI, AMIR. Effect of temperature on the shaping process of an extruded wood-plastic composite (WPC) profile in a novel post-production process. 2017. Diss.

**766.** LAAKKONEN, JUSSI. An approach for distinct information privacy risk assessment. 2017. Diss.

**767.** KASURINEN, HELI. Identifying the opportunities to develop holistically sustainable bioenergy business. 2017. Diss.

**768.** KESKISAARI, ANNA. The impact of recycled raw materials on the properties of wood-plastic composites. 2017. Diss.

**769.** JUKKA, MINNA. Perceptions of international buyer-supplier relational exchange. 2017. Diss.

**770.** BAYGILDINA, ELVIRA. Thermal load analysis and monitoring of doubly-fed wind power converters in low wind speed conditions. 2017. Diss.

**771.** STADE, SAM. Examination of the compaction of ultrafiltration membranes with ultrasonic time-domain reflectometry. 2017. Diss.

**772.** KOZLOVA, MARIIA. Analyzing the effects of a renewable energy support mechanism on investments under uncertainty: case of Russia. 2017. Diss.

**773.** KURAMA, ONESFOLE. Similarity based classification methods with different aggregation operators. 2017. Diss.

**774.** LYYTIKÄINEN, KATJA. Removal of xylan from birch kraft pulps and the effect of its removal on fiber properties, colloidal interactions and retention in papermaking. 2017. Diss.

**775.** GAFUROV, SALIMZHAN. Theoretical and experimental analysis of dynamic loading of a two-stage aircraft engine fuel pump and methods for its decreasing. 2017. Diss.

**776.** KULESHOV, DMITRII. Modelling the operation of short-term electricity market in Russia. 2017. Diss.

**777.** SAARI, JUSSI. Improving the effectiveness and profitability of thermal conversion of biomass. 2017. Diss.

**778.** ZHAO, FEIPING. Cross-linked chitosan and β-cyclodextrin as functional adsorbents in water treatment. 2017. Diss.

**779.** KORHONEN, ILKKA. Mobile sensor for measurements inside combustion chamber – preliminary study. 2017. Diss.

**780.** SIKIÖ, PÄIVI. Dynamical tree models for high Reynolds number turbulence applied in fluid-solid systems of 1D-space and time. 2017. Diss.

**781.** ROMANENKO, ALEKSEI. Study of inverter-induced bearing damage monitoring in variable-speed-driven motor systems. 2017. Diss.

**782.** SIPILÄ, JENNI. The many faces of ambivalence in the decision-making process. 2017. Diss.